Title

The Search for Novel Superconductivity in Inhomogeneous Materials using Magnetic Field Modulated Microwave Spectroscopy

Author

Wampler, James Paris

Publication Date

2019

Peer reviewed|Thesis/dissertation

UNIVERSITY OF CALIFORNIA SAN DIEGO

The Search for Novel Superconductivity in Inhomogeneous Materials using Magnetic Field Modulated Microwave Spectroscopy

A dissertation submitted in partial satisfaction of the

requirements for the degree Doctor of Philosophy

in

Physics

by

James Paris Wampler

Committee in charge:

Professor Ivan K. Schuller, Chair
Professor Eric E. Fullerton
Professor Olivia A. Graeve
Professor M. Brian Maple
Professor Oleg G. Shpyrko

2019

The Dissertation of James Paris Wampler is approved, and it is acceptable in quality and form for publication on microfilm and electronically:

_____

_____

_____

_____

_____

Chair

University of California San Diego

2019

EPIGRAPH

"[Phase] [s]pace is big. Really big. You just won't believe how vastly, hugely, mind-bogglingly big it is."

-Douglas Adams, *The Hitchhiker's Guide to the Galaxy*

TABLE OF CONTENTS

LIST OF FIGURES

LIST OF TABLES

ACKNOWLEDGEMENTS

This PhD has been a long time coming and was not exactly what I imagined when I applied for grad school while finishing my undergraduate work at Wesleyan University. I did not have a much lab experience at the time and in truth, did not know what I was in for. Despite that, this has been a rewarding experience in which I have grown in so many ways. Many people have helped me and taught me along the way and among them all, I would first like to thank my advisor, Ivan Schuller. He was not just an excellent research advisor, he also taught me many invaluable life skills. He taught me to slow down when I'm talking and say only what I mean to say. He taught me not to overcomplicate, to put agreements in writing and to give a good presentation. His guidance and his 13 rules have helped me grow immeasurably.

I would like to thank my family. My father, Jim Wampler, my mother, Marilyn Stelzner, and my sister Claire. My parents encouraged my interest in math games as well as soccer and piano. They sent me to Peninsula School where I grew up as a person and to Wesleyan University where I developed my love of physics. They have always been there for me when I needed someone. My sister is one of my best friends and in between friendly teasing, she's always been encouraging. Claire, I promise, now I can come and visit you in New York a little bit more often.

I'd like to thank my girlfriend, Sarah Matteson. Sarah, thank you for all your patience through this long, long process. When we first met, I told you (very, very optimistically) that I guessed I had about 6 months left in my PhD. Now that I'm finishing two years later, it's pretty clear that my guess was a little bit off. She teased me when I needed it and encouraged me when the journey seemed longest and most stressful.

Finally, I would like to thank all the members of the Schuller lab who I worked with over the years. Dr. Thomas Saerbeck guided me as a researcher when I joined Professor Schuller's

lab. At the time, I had very little experience in a lab and Thomas was my Yoda. He taught me numerous experimental techniques and coached me in my early projects. I worked with Dr. Juan Gabriel Ramírez and Dr. Ali Basaran on several MFMMS projects. Early in my PhD, they helped teach me to work in the lab and later on, we worked well together on several different projects. In the middle of my PhD, there was a time when Dr. Christian Urban and Dr. Ilya Valmianski and I were the only three members of the lab. We worked together and had many fruitful discussions.

Chapter 1 was in part prepared using material submitted for publication: Wampler, James; Hojem, Alex; Schuller, Ivan K. "Search Faster, Not Smarter: Using Microwaves to Search for New Superconductors." J. W. was the principal researcher/author on this paper.

Chapter 2 was prepared based on material submitted for publication: Wampler, James; Thiemens, Mark; Cheng, Shaobo; Zhu, Yimei; Schuller, Ivan K. "Natural Superconductivity Found in Meteorites." J. W. performed the experiments, M.T. provided the meteorites and I.K.S. supervised the project. S.C. conducted the TEM experiments under the supervision of Y. Z.. All authors contributed to the data analysis and writing of the manuscript. J. P. W. was the principal researcher/author on this paper.

Chapter 3 was prepared based on material that is to be submitted for publication: Wampler, James; Hua, Nelson; Kukreja, Roopali; Ramirez, Juan Gabriel; Basaran, Ali; Fullerton, Eric; Shpyrko, Oleg; Schuller, Ivan K. "The Electromagnetic Origin of the Microwave Absorption Response of Fe3O4 Thin Films." J. W. was the principal researcher/author on this paper.

Chapter 4 was prepared based on coauthored unpublished material with the following author list: Wampler, James; Trastoy, Juan; Schuller, Ivan K. J. W. was the principal researcher/author for this work.

VITA

Education

September 2012 – September 2019	Ph.D Physics	University of California San Diego
September 2011 – September 2012	M.S. Physics	University of California San Diego
September 2007 – June 2011	B.A. Physics, Math with Honors	Wesleyan University

Publications

1. **Wampler, James;** Thiemens, Mark; Cheng, Shaobo; Zhu, Yimei; Schuller, Ivan K. "Natural Superconductivity Found in Meteorites" (submitted for publication)
2. **Wampler, James;** Hua, Nelson; Kukreja, Roopali; Ramirez, Juan Gabriel; Basaran, Ali; Fullerton, Eric; Shpyrko, Oleg; Schuller, Ivan K. "The Electromagnetic Origin of the Microwave Absorption Response of Fe_3O_4 Thin Films" (manuscript in preparation)
3. **Wampler, James;** Hojem, Alex; Schuller, Ivan K. "Search Faster, Not Smarter: Using Microwaves to Search for New Superconductors" J. Wampler, A. Hojem, I. Schuller, in *Proc.Int.Symp. "Superconductivity & Pressure: A Fruitful Relationship on the Road to Room Temperature Superconductivity."* May 21-22, 2018. CERA, Ed. (Madrid, Spain) *(in press 2019)*
4. Guénon, Stefan; Ramírez, Juan Gabriel; Basaran, Ali C.; **Wampler, James**; Thiemens, Mark; Schuller, Ivan K. Search for New Superconductors: an Electro-Magnetic Phase Transition in an Iron Meteorite Inclusion at 117 K. *J. Supercond. Nov. Magn.* **30**, 297–304 (2017).
5. Guénon, Stefan; Ramírez, Juan Gabriel; Basaran, Ali C.; **Wampler, James**; Thiemens, Mark; Taylor, Susan; Schuller, Ivan K. Search for superconductivity in micrometeorites. *Sci. Rep.* **4**, 7333 (2014).
6. Saerbeck, Thomas; Pereiro, Juan; **Wampler, James**; Stanley, Jacob; Wingert, James; Shpyrko, Oleg G.; Schuller, Ivan K. Ferromagnetism in partially oxidized CuCl. *J. Magn. Magn. Mater.* **346**, 161–165 (2013).

ABSTRACT OF THE DISSERTATION

The Search for Novel Superconductivity in Inhomogeneous Materials using Magnetic Field Modulated Microwave Spectroscopy

by

James Paris Wampler

Doctor of Philosophy in Physics

University of California San Diego, 2019

Professor Ivan K. Schuller, Chair

Most major discoveries of high temperature superconductors have not been predicted by theory. While theory can explain experimental findings and motivate ideas of where do search, it does not reliably predict new superconductors. Instead, the best way to find new superconductors is to synthesize many materials and test them. Measuring inhomogeneous samples speeds up this process, allowing the simultaneous testing of several material phases. However, since potential

superconducting phases in such samples could be minute, it is necessary to use magnetic field modulated microwave spectroscopy (MFMMS), which is three orders of magnitude more sensitive than conventional magnetometry techniques. MFMMS is used as a first detection method and superconducting samples can be subsequently studied with other measurement techniques. Using MFMMS, superconductivity was detected inside of two meteorite samples and further characterized as an alloy of lead, indium and tin. This is the first detection of extraterrestrial superconducting samples and is significant due to the possibility that these and similar samples could have been superconducting in their natural environment. In addition, MFMMS was used to study chemically doped Sr_2IrO_4 powder samples. While the superconducting phase detected is likely a known superconductor, $SrIr_2$, this demonstrates this technique's advantages over conventional magnetometry, which did not measure a superconducting transition. Finally, this dissertation discusses techniques to analyze non-superconducting phase transitions using magnetic hysteresis loops and magnetoresistance measurements. These techniques allows for a more thorough understanding of these transitions, which increases the ability to use MFMMS to characterize unknown phase transitions in homogeneous and inhomogeneous samples.

Chapter I - Introduction

1.1 Motivation

Since the first discovery of superconductivity (*1*), there have been continued efforts to find materials with higher and higher superconducting critical temperatures. However, despite sustained interest, most major discoveries of high temperature superconductors have not been predicted by theory (*2–4*). While theory explains much of the experimental results quite successfully, it has not been successful in predicting which material phases will be superconducting. Theory can motivate ideas of where to search for superconductivity, but currently, the best way to find new superconducting phases is to search compounds similar to existing superconductors, or to synthesize material phases one at a time and be lucky enough to find a new superconductor. One way to mitigate this is to search faster, by testing a large number of material phases. This is difficult to do synthesizing different material phases one at a time. However, by measuring inhomogeneous samples, we can search for superconductivity in many material phases simultaneously, which can drastically speed up the search. This is a historically proven approach: for instance, the original discovery of superconductivity in the Y-Ba-Cu-O system was in a multiphase sample (*5*).

Although measuring inhomogeneous samples is an effective way of increasing the odds of producing a new superconductor, characterizing them is inherently difficult because a superconducting phase can be a very small fraction of the overall sample. An extremely sensitive technique is required to detect such phases. Magnetic field modulated microwave spectroscopy (MFMMS) is the most sensitive experimental technique for detecting superconducting transitions within inhomogeneous materials (*6*). The MFMMS apparatus can detect as little as 10^{-12} cc of superconducting material in a non-superconducting matrix between 4 K and 300 K, within one

hour. This is three orders of magnitude more sensitive than conventional detection methods such as a superconducting quantum interference device (SQUID) magnetometry or vibrating sample magnetometry (VSM). In addition, because this technique selectively measures changes in electromagnetic properties, it measures minimal signal from "uninteresting" (i.e. non-superconducting) phases. This sensitivity and selectivity allows it to detect minute superconducting phases embedded in heterogeneous samples.

The rest of this chapter will discuss the MFMMS technique, different measurement routines that are useful when taking MFMMS measurements, complementary techniques that can be used in conjunction with MFMMS and different inhomogeneous samples that have been measured with MFMMS. The rest of this dissertation will discuss different samples measured using MFMMS in conjunction with other measurement techniques. Chapter 2 will discuss the discovery of natural superconductivity within two meteorite samples. Chapter 3 will discuss MFMMS measurements of Fe_3O_4 thin films and a computational technique that can be used to model and analyze electromagnetic phase transitions using the MFMMS. The analysis presented is useful in analyzing a broad range electromagnetic phase transitions, which helps to distinguish different phase transitions observed within inhomogeneous samples. Chapter 4 will discuss a search for superconductivity within doped Sr_2IrO_4 polycrystalline powder samples that are synthesized using powder metallurgy.

1.2 MFMMS Background and Measurement Techniques

MFMMS is a microwave absorption technique similar to electron paramagnetic resonance (EPR) spectroscopy. In the MFMMS technique, samples are inserted into a microwave cavity with a small applied AC magnetic field (typically 15 Oe) and a DC offset magnetic field (up to 1 T). In contrast to EPR, these fields are oriented in parallel to the microwave magnetic

field, which suppresses the resonant signal. In addition, while EPR is typically capable only of making isothermal DC magnetic field scans, MFMMS can also make temperature scans with fixed DC field. MFMMS measures *dP/dh*, where *h* is the applied magnetic field and *P* is the microwave power absorbed in the system (*6*).

MFMMS can be effectively used to measure the superconducting transitions of material phases within samples. When measuring a superconducting sample with a temperature sweep, the AC magnetic field H_{AC} forces the sample into and out of the superconducting phase as the temperature crosses T_c (Fig. 1.1). The microwave power absorbed changes drastically across the superconducting transition resulting in a peak in the MFMMS signal, *dP/dh*, across the superconducting transition. The onset of this peak is at the critical field, $H_c(T)$ of a type 1 superconductor or $H_{c2}(T)$ of a type 2 superconductor. This occurs because for metallic and superconducting samples, the power absorbed is expressed as:

$$P = \frac{1}{2}\iint R_S(T,\omega)h_{mw}^2 dA \,, \tag{1.1}$$

where R_S is the surface resistance, T is the temperature, ω is the microwave frequency, and h_{mw} is the microwave magnetic field (*6*). For a given material phase, the argument of the surface integral is constant and so $P \propto R_S$. Because the surface resistance of a material changes drastically across a superconducting transition, so does the microwave power absorbed in a cavity.

The MFMMS is an additive technique, meaning that in a multiphase sample, the signal of each individual phase is added together. As a result, superconducting peaks can be easily detected even when the superconducting phase is only a minority of the overall sample.

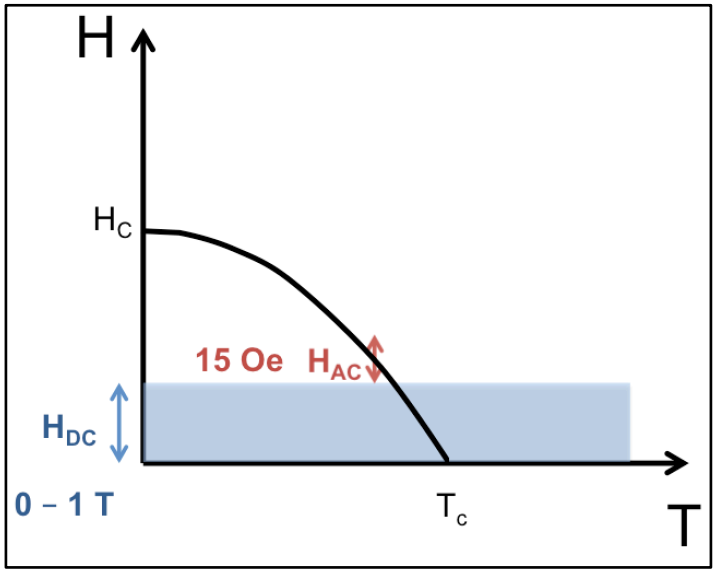

Figure 1.1: Sketch of a superconducting phase diagram. In black is a superconducting phase diagram. For a type I superconductor, the critical temperature $T_c(H = 0$ Oe*)* is indicated by T_c and the critical field $H_c(T = 0$ K) is indicated by H_c. For a type II superconductor, H_c would indicate $H_{c2}(T = 0$ K). Blue indicates the DC magnetic field applied to the sample, which is constant during a temperature sweep and ranges from 0 – 1 T. Red indicates the AC field applied in addition to the DC field, which can cross the superconducting phase boundary.

This peak in the MFMMS signal is characteristic of a superconducting transition: all superconducting transitions measured in temperature sweeps in the MFMMS have produced such a peak (Fig. 1.2a, for example). However, there is at least one non-superconducting material, (Ga,Mn)As (*7*), that has been shown to cause a peak in the MFMMS signal (*6*) (Fig 1.2b). While the peak in the MFMMS signal produced by this material's ferromagnetic transition is similar to one produced by a superconducting transition, two types of complementary measurements in the MFMMS can be used to distinguish between these sorts of samples.

The first method of distinguishing superconducting peaks in the MFMMS from non-superconducting peaks is to make isothermal DC field sweep loops in the MFMMS. Field sweep loops are performed by measuring first with increasing and then decreasing DC fields, at a fixed temperature. The chirality of this signal can be used as a signature of superconductivity. Superconductors have been shown to have clockwise chirality (Fig 1.2c). No non-

superconducting material with a peak in the MFMMS has been shown to have clockwise chirality. (Ga,Mn)As does not have any chirality (Fig 1.2d) and in general, magnetic materials do not necessarily exhibit chirality in the MFMMS.

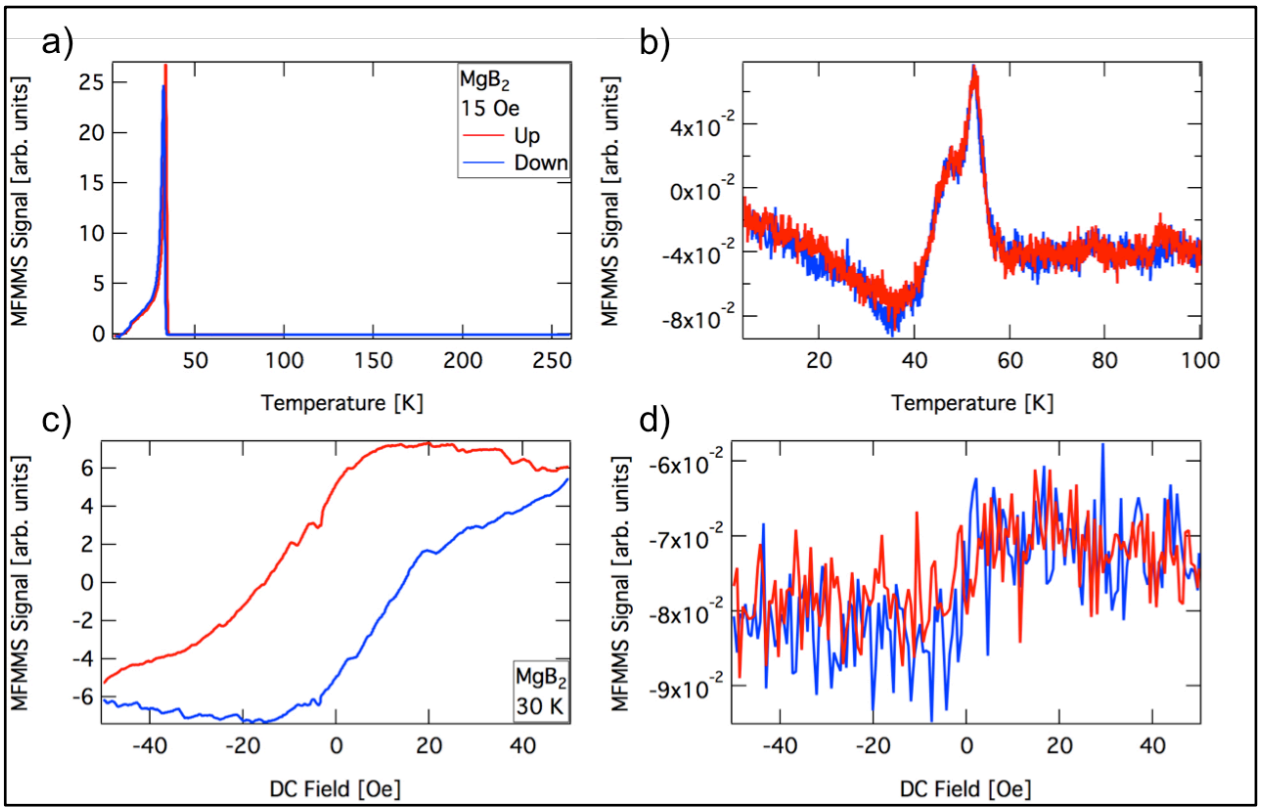

Figure 1.2: MFMMS temperature sweep measurements of MgB_2 (a) and (Ga,Mn)As (b). MFMMS field sweep measurements of MgB_2 (c) and (Ga,Mn)As (d). Red curves indicate increasing temperature or field, blue indicates decreasing temperature or field.

In addition to the chirality, the shape of superconducting field sweep loops have been found to have several distinguishing features (*8*). Asymmetric field sweep loop measurements were taken on a range of different superconducting materials to study these similarities. In these measurements, the DC field was scanned back and forth twice between -50 Oe and 600 Oe. These measurements were taken on a range of superconducting powder samples: MgB_2, Nb, YBCO and Nb_3Sn (Fig 1.3a-d). Similar measurements were taken for comparison on non-superconducting powder samples, including Fe_9S_{10} and (Ga,Mn)As (Fig 1.3e,f). In each of the

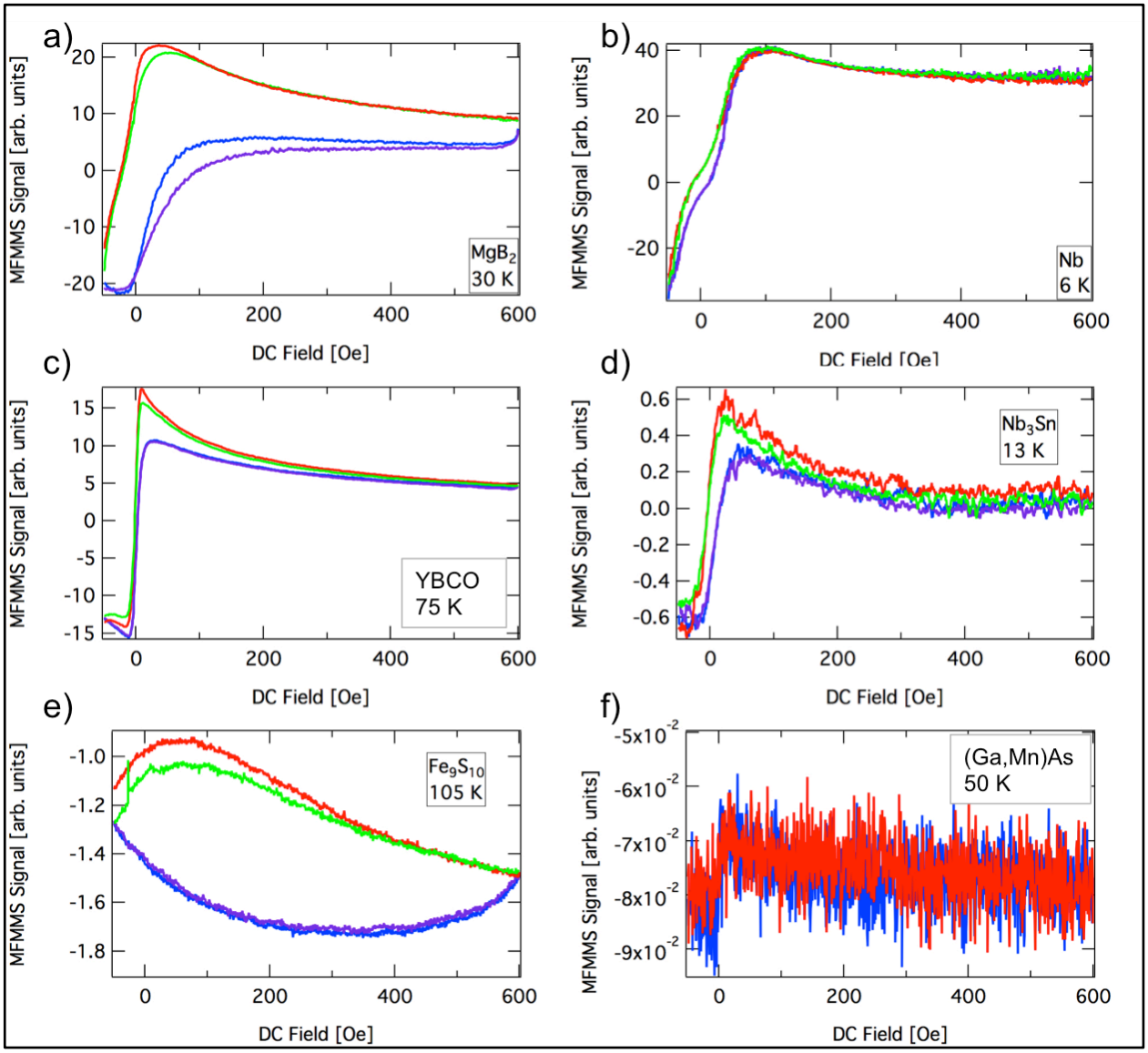

Figure 1.3: MFMMS asymmetric field sweep measurements of MgB_2 (a), Nb (b), YBCO (c), Nb_3Sn (d), Fe_9S_{10} (e) and (Ga,Mn)As (f). Red indicates increasing field, blue indicates decreasing field. For all measurements except that of (Ga,Mn)As, green indicates a second sweep with increasing field, purple indicates a second sweep with decreasing field.

superconducting samples, there is a roughly linear region of the MFMMS signal around 0 Oe DC field, with a positive slope as the DC field is increased. This linear region terminates in a peak at low, positive DC field. Above this peak, the MFMMS signal has negative slope but remains positive. There is a training effect between the loops so that the second loop has a reduced MFMMS signal with increasing DC field. While individual features can be seen in field sweeps

of other materials (Fig. 1.3e), the complete set of features is unique to superconducting samples and is characteristic of superconductivity. In other words, all superconducting samples measured showed this set of features and no non-superconducting samples did.

This linear region, peak and then negative slope in the MFMMS signal in superconducting field sweep loops occurs because of the behavior of the surface resistance within the superconducting regime. As previously discussed, in metallic and superconducting samples, the surface resistance R_S is proportional to the power absorbed, P and therefore dR_S/dH is proportional to the MFMMS signal, dP/dH. At sufficiently low fields, R_S is a function of H^2. This means that dR_S/dH is a linear function of H, which explains the approximately linear MFMMS signal (*9*). At higher fields above $H_{c1}(T)$, R_S is a function of $H^{1/2}$. This means that dR_S/dH is a function of $H^{-1/2}$ which explains the MFMMS signal's shape and negative slope (*10*).

The second method of distinguishing superconducting peaks in MFMMS temperature sweeps from non-superconducting ones is to study the evolution of temperature sweep data with increasing DC fields. Measurements of Nb thin films have shown that at sufficiently high fields, the peak is suppressed in both onset temperature and magnitude (*6*). This behavior has not been seen in non-superconducting samples. Notably, in addition to distinguishing superconducting transitions, this technique also allows the investigation of the temperature evolution of $H_{c2}(T)$, which can be accomplished by plotting the onset temperature of the superconducting peak as a function of field.

1.3 Inhomogeneous Samples

There are several different types of inhomogeneous samples that can be efficiently searched for novel superconductivity, each presenting their own advantages and limitations. Synthetic powder samples are created through powder metallurgy. This method, explored more

fully in chapter 4, involves mixing powders and then heating them under specific atmospheres. Inhomogeneous samples can be created using this technique with significantly less effort that it takes to achieve a pure phase. The downside of powder samples is that if superconductivity is discovered within an inhomogeneous sample, it can be nontrivial to identify the superconducting phase from within the bulk of the sample. Copper chloride powder samples have been previously studied in the MFMMS using these techniques (*11*).

Inhomogeneous thin film samples can be synthesized by creating phase spread alloys, which are thin film samples with two or three materials sputtered off center from one another so that the resultant sample has a gradient of phase concentrations. While it can be more difficult to successfully grow such samples than it is to create powder samples, it is much easier to isolate the superconducting phase if one is detected. Since the phase spread alloy has a gradient of phase concentration, different phases are spatially separated from each other, so the sample can simple be broken into pieces and each piece characterized separately. La-Si-C Phase spread alloys have been previously synthesized and studied in the MFMMS (*12*).

While both synthetic powder samples and phase spread alloys allow for the efficient synthesis of a large number of phases, sample synthesis is still a difficult step that can be a bottleneck in finding new superconductors. One way to circumvent this difficulty is to measure natural samples. These can range from natural minerals to extraterrestrial samples such as meteorites. While measuring natural samples negates the necessity of sample synthesis, there are a few limitations. First, natural samples are prepared typically by scraping powder material from a larger bulk sample, meaning that all of the limitations in measuring synthesized powder restrict the measurement of natural samples as well. Second, while natural samples contain a range of material phases, there are still many phases that do not form naturally, which restricts what parts

of material phase space can be explored. Finally, many material phases do not exist naturally as minerals, and so can not be studied in this way. Extraterrestrial materials are a category of natural sample that present unique advantages for searching for superconductivity. In contrast with terrestrial samples, they can form in much more extreme synthesis conditions, including temperature, pressure and cooling time, meaning that phases can form that might not form naturally in a terrestrial environment. Chapter 2 presents the discovery of Pb-Sn-In superconducting material in two meteorite samples. Several extraterrestrial samples have been previously studied using MFMMS, including micrometeorites (*13*), meteorites (*14*) and lunar rock, brought back to the earth by the Apollo 17 mission. This last research showed that the moon is not, in fact, a superconductor.

1.4 Measuring Inhomogeneous Samples in MFMMS

When searching for superconductivity in inhomogeneous materials, MFMMS is an ideal first detection technique, but in order to thoroughly analyze potentially superconducting samples, complementary techniques are necessary. However, many of these techniques, such as vibrating sample magnetometry (VSM), x-ray diffraction analysis (XRD) and energy-dispersive x-ray spectroscopy (EDX) are not well suited for measuring highly inhomogeneous samples. Therefore, in order to prepare samples for further analysis, it is necessary to prepare subsamples with higher concentrations of the superconducting phase within them. When working with powder samples (including natural samples), this is accomplished by performing a “divide and conquer” process. This process allows the isolation of the powder grains with the largest superconducting fraction, which in turn makes further analysis feasible.

In performing a divide and conquer procedure, an inhomogeneous sample containing a superconducting phase (termed the “parent sample”) is divided into subsamples. This division is

typically done by examining the sample under the microscope and sorting out different grains based on their visual morphology (ie: what they look like). Each subsample must then be measured using MFMMS temperature sweeps. If the subsamples contain substantially different quantities of superconducting material (which is judged by the height of the superconducting peak in the MFMMS signal), then the grains containing higher percentage of superconducting material have been isolated from those containing less. This is repeated as necessary, further subdividing subsamples, if there are sufficiently different grains of powder within a given subsample. Conversely, if the various subsamples do not contain substantially different quantities of the superconducting phase, then the process did not accomplish anything. It should be noted that the rigor of this method comes entirely from the subsequent measurements and not the initial separation.

Once the parent sample has been separated into different subsamples with varying quantities of superconducting material, it is necessary to measure all of these subsamples with the aforementioned complementary measurement techniques. By doing this, the subsamples with little or no superconducting material can be compared to those with a significant quantity; any similarities are likely unrelated to the superconducting phase, while any differences could be related. By measuring these subsamples with a barrage of different tests, it is usually possible to deduce the likely superconducting phase. Once that is done, synthesis can be attempted on a pure phase sample of that material, to confirm the superconductivity.

1.5 Acknowledgements

Chapter 1 was in part prepared using material submitted for publication: Wampler, James; Hojem, Alex; Schuller, Ivan K. “Search Faster, Not Smarter: Using Microwaves to Search for New Superconductors.” J. W. was the principal researcher/author on this paper.

1.6 References

1. H. K. Onnes, The Superconductivity of Mercury. *Comm. Phys. Lab. Univ., Leiden*. **122**–**124** (1911).

2. J. G. Bednorz, K. A. Müller, Possible High T_c Superconductivity in the Ba-La-Cu-O System. *Zeitschrift für Phys. B*. **64**, 189 (1986).

3. J. Nagamatsu, N. Nakagawa, T. Muranaka, Y. Zenitani, J. Akimitsu, Superconductivity at 39 K in Magnesium Diboride. *Nature*. **410**, 63 (2001).

4. Y. Kamihara, T. Watanabe, M. Hirano, H. Hosono, Iron-based layered superconductor $La[O_{1-x}F_x]FeAs$ (x= 0.05-0.12) with T_c = 26 K. *J. Am. Chem. Soc.* **130**, 3296 (2008).

5. M. K. Wu, J. R. Ashburn, C. J. Torng, P. H. Hor, R. L. Meng, L. Gao, Z. J. Huang, Y. Q. Wang, C. W. Chu, Superconductivity at 93 K in a New Mixed-Phase Y-Ba-Cu-O Compound System at Ambient Pressure. *Phys. Rev. Lett.* **58**, 908 (1987).

6. J. G. Ramírez, A. C. Basaran, J. de la Venta, J. Pereiro, I. K. Schuller, Magnetic field modulated microwave spectroscopy across phase transitions and the search for new superconductors. *Reports Prog. Phys.* **77**, 093902 (2014).

7. H. Ohno, A. Shen, F. Matsukura, A. Oiwa, A. Endo, S. Katsumoto, Y. Iye, (Ga,Mn)As: A new diluted magnetic semiconductor based on GaAs. *Appl. Phys. Lett.* **69**, 363 (1996).

8. K. W. Blazey, K. A. Müller, J. G. Bednorz, W. Berlinger, Low-field microwave absorption in the superconducting copper oxides. *Phys. Rev. B*. **36**, 7241 (1987).

9. J. Halbritter, On Surface Resistance of Superconductors. *Zeitschrift für Phys.* **266**, 209 (1974).

10. F. J. Owens, C. P. J. Poole, in *Electromagnetic Absorption in the Copper Oxide Superconductors* (Kluwer Academic Publishers, New York, Boston, Dordrecht, London, Moscow, 1999), pp. 143–144.

11. T. Saerbeck, J. Pereiro, J. Wampler, J. Stanley, J. Wingert, O. G. Shpyrko, I. K. Schuller, Ferromagnetism in partially oxidized CuCl. *J. Magn. Magn. Mater.* **346**, 161 (2013).

12. J. de la Venta, A. C. Basaran, T. Grant, A. J. S. Machado, M. R. Suchomel, R. T. Weber, Z. Fisk, I. K. Schuller, Methodology and search for superconductivity in the La–Si–C system. *Supercond. Sci. Technol.* **24**, 075017 (2011).

13. S. Guénon, J. G. Ramírez, A. C. Basaran, J. Wampler, M. Thiemens, S. Taylor, I. K. Schuller, Search for superconductivity in micrometeorites. *Sci. Rep.* **4**, 7333 (2014).

14. S. Guénon, J. G. Ramírez, A. C. Basaran, J. Wampler, M. Thiemens, I. K. Schuller, Search for New Superconductors: an Electro-Magnetic Phase Transition in an Iron Meteorite Inclusion at 117 K. *J. Supercond. Nov. Magn.* **30**, 297 (2017).

Chapter 2 – Natural Superconductivity Found in Meteorites

2.1 Introduction

Meteorites contain a wide range of material phases due to the extreme environments found in space and are ideal candidates to search for natural superconductivity. They can preserve the oldest phases in the solar system (*1*), which can form under hundreds of GPa of pressure (*2*) with typical crystallization temperatures of 500-700 °C (*3*). In addition, they can have cooling rates of 100-10,000 °C/Myr. Because of this, meteorites (particularly those with extreme formation conditions) can contain material phases such as quasicrystals, which are not found in terrestrial environments (*4*). Past studies of extraterrestrial materials have led to new, previously unpredicted insights (*5*–*7*). However, meteorites are chemically inhomogeneous and superconducting phases in them could potentially be minute, rendering detection of these phases difficult. To alleviate this difficulty, we have studied them with the ultrasensitive Magnetic Field Modulated Microwave Spectroscopy (MFMMS) technique (*8*). Here, we report the identification of superconducting phases in two meteorites, Mundrabilla, a group IAB iron meteorite (*9*) and GRA 95205, a ureilite (*10*). MFMMS measurements of each meteorite detected superconducting transitions with critical temperatures above 5 K. By subdividing and re-measuring individual samples, grains containing the largest superconducting fraction were isolated. Subsequent measurements and analysis identified the likely phases as alloys of lead, indium and tin. To our knowledge, these are the first observed superconducting extraterrestrial materials.

Both Mundrabilla and GRA 95205 are nonchondritic meteorites (they do not possess glassy chondrules). Nonchondritic meteorites have been melted and recrystallized in their history and do not preserve an original record of the pre-solar interstellar medium (*1*). Mundrabilla is an iron meteorite, a class of metal meteorites formed largely from melting in asteroidal cores. It is

an FeS-rich meteorite with extremely slow cooling times, estimated to be 3 °C/yr (*11*, *12*). GRA 95205 is a ureilite meteorite that was heavily shocked during formation (*13*). Ureilites are primitive (meaning that they are nearly chondritic chemical composition) and largely composed of olivine. Meteorites with extreme formation conditions are ideal for observing exotic chemical species, such as superconductors.

MFMMS can measure 10^{-12} cm^3 of superconducting material. This sensitivity is critical in measuring possible minute phases within inhomogeneous materials (*8*). MFMMS has previously been used to search for novel superconductivity in several types of inhomogeneous samples, such as phase spread alloys (*14*), bulk samples (*15*) and even natural samples, including meteorites (*16*, *17*). However, previous searches for superconductivity in meteorites have not identified any superconducting compounds.

2.2 Measurement

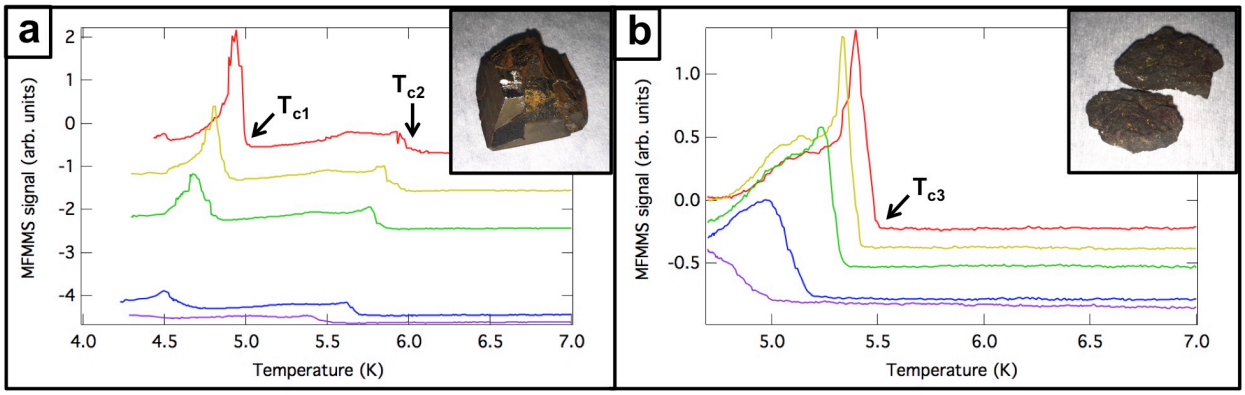

Figure 2.1: MFMMS temperature sweeps of samples from (a) Mundrabilla sample MUND-1 and (b) GRA 95205 sample GRA-1. These sweeps are performed with a DC field, H_{DC} set to 15 Oe (red), 100 Oe (yellow), 200 Oe (green), 500 Oe (blue), and 1000 Oe. An AC field, H_{AC} = 15 Oe is applied in parallel to the DC field.

MFMMS measurements were made on a powder sample extracted from Mundrabilla (MUND-1). At low DC field, H_{DC} = 15 Oe, there are sharps transition at T_{c1} = 5 K and T_{c2} = 6 K that indicates superconducting transitions (Fig. 2.1a). By applying increasing DC fields, these

peaks are suppressed in both temperature and in magnitude and are barely visible at H_{DC} = 1000 Oe. This peak shape and field evolution are characteristic of a superconducting transition (*8*). Peaks in the MFMMS signal were observed in five of the ten samples collected from this meteorite.

Similar MFMMS measurements were made of a sample extracted from a piece of GRA 95205 (GRA-1). When the applied DC field (H_{DC}) is 15 Oe, there is a peak at T_{c3} = 5.5 K, and increasing H_{DC} suppresses this transition in temperature and magnitude (Fig. 2.1b), just like Mundrabilla. Only one of six samples taken from this meteorite exhibited such a peak.

In order to confirm that the peaks observed in MFMMS indicated superconductivity, Vibrating-Sample Magnetometry (VSM) measurements were performed on samples from Mundrabilla (Fig. 2.2). Zero-field cooled (ZFC) measurements of sample MUND-1 showed a strong diamagnetic response, characteristic of a superconducting transition (Fig. 2.2a). This diamagnetic response was suppressed in onset temperature and in magnitude at increased DC fields (Fig. 2.2b). In addition, the curves show multiple inflection points, which are likely the result of the multiple superconducting transitions observed in MFMMS. Low magnetic field ZFC and field cooled (FC) measurements (5 Oe and 10 Oe, Fig. 2.2c) showed similar behavior. The weaker response observed in FC measurements is consistent with superconductivity. The onset temperature for the superconducting transition observed with the VSM is ~1 K higher than the onset temperature observed using MFMMS, which is within the temperature uncertainty for the flow cryostat used in MFMMS and is likely a thermal lag typical of that technique.

In order to calculate the average magnetic susceptibility, the volume of the samples has been estimated from 2D images using image-processing software ($V_{MUND-1} = 9.10 \times 10^{-5} \pm 7.99 \times 10^{-5}$ cm^3 and $V_{MUND-2} = 8.06 \times 10^{-4} \pm 5.40 \times 10^{-4}$ cm^3). Using this volume, low magnetic field

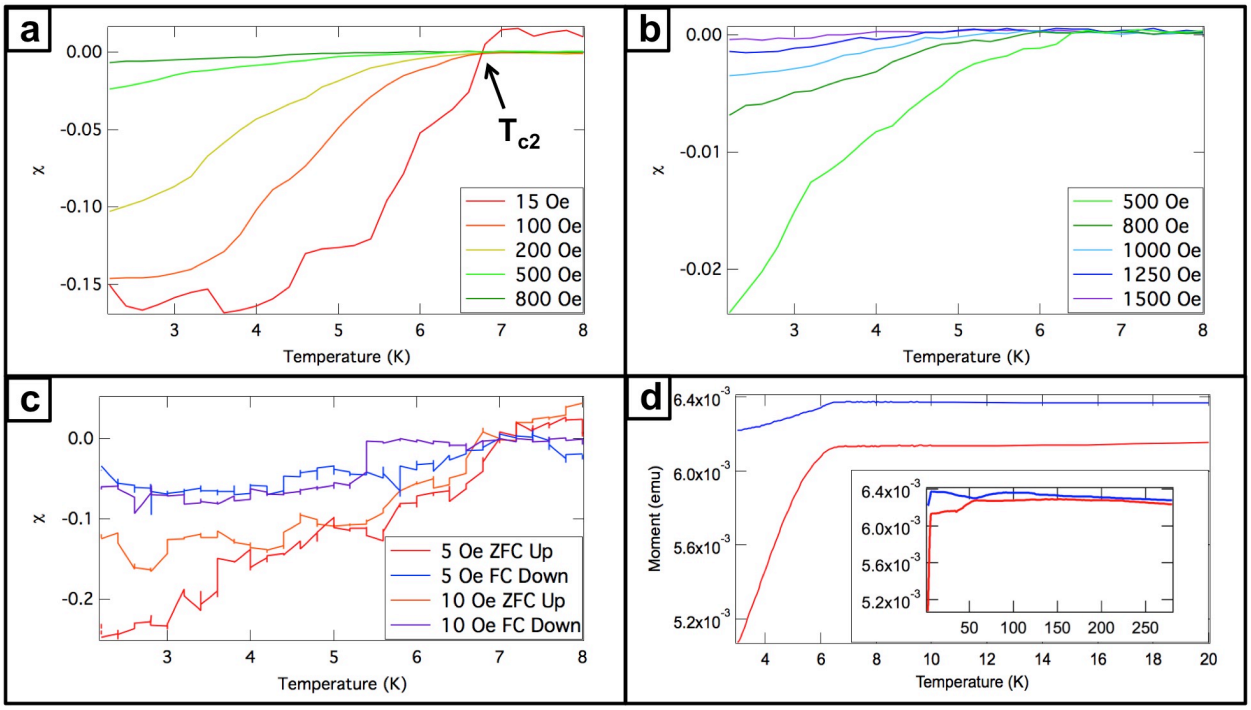

Figure 2.2: VSM measurements of samples from Mundrabilla. ZFC measurements on sample MUND-1 were performed with applied magnetic field ranging from 15-1500 Oe. Measurements from 15-800 Oe (a) and 500-1500 Oe (b) shown separately for visual clarity. FC and ZFC measurements at 5 Oe and 10 Oe were taken with multiple consecutive data taken at each temperature (c). All measurements offset for visual clarity. ZFC measurements (red) and FC measurements (blue) were performed on a second sample, MUND-2, with an applied magnetic field of 500 Oe (d). Inset shows full temperature range.

measurements (Fig. 2.2c) give a superconducting volume fraction across the whole sample of approximately 5%. Measurements on another sample from Mundrabilla (MUND-2) showed a similar transition (Fig. 2.2d), in addition to other magnetic behavior observed at higher temperatures.

Since samples from both meteorites contain superconducting phases, we performed a "divide and conquer" process to isolate individual grains that contain the largest superconducting fractions. This isolation allows us to determine their chemical composition. We examined the samples (denoted as "parent samples") with an optical microscope and completely divided them based on their visual morphology (ie: what the samples looked like) into different subsamples. If

the strength of the superconducting response is substantially depends on the visual morphology, then these subsamples could be subjected to a battery of further tests.

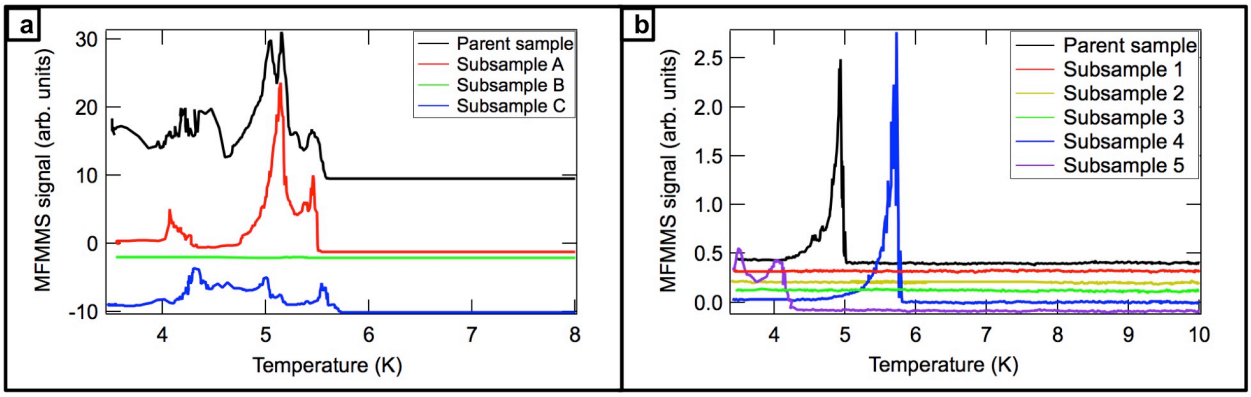

Figure 2.3: MFMMS temperature sweeps of divide and conquer samples. These measurements are performed with $H_{DC} = H_{AC} = 15$ Oe for parent samples and subsamples from the (a) Mundrabilla meteorite and (b) GRA 95205. The data is vertically offset for visual clarity.

MFMMS data was taken from a parent sample collected from Mundrabilla (sample MUND-2, Fig. 2.3a) and the subsamples derived from the divide and conquer process. Under the microscope, there were three visually distinct morphologies that were separated into subsamples A, B and C. Subsample A contained grains that were apparently metallic and homogenous. Subsample B contained samples that appeared non-reflective, with colors ranging from oranges to dark browns. Subsample C contained samples that appeared inhomogeneous and partially metallic.

Subsample A showed the strongest superconducting response in MFMMS, subsample B showed a slight superconducting response and subsample C showed a moderate response. Thus, the more metallic the sample appeared, the stronger the superconducting response. Further, the small response from subsample B indicates that almost all of the superconducting material is in grains that have metallic luster. The phases responsible for the superconductivity are then likely to be the macroscopic phases responsible for the luster of the grains.

Similar divide and conquer data measurements were performed on samples from GRA 95205 (Fig. 2.3b). The parent sample (taken from sample GRA-1) was divided into subsamples 1 through 5. Subsample 1 contained black grains, subsample 2 contained semi-translucent grains and subsample 3 was brown and stony. Subsample 4 was white and crumbly with apparently metallic inclusions and subsample 5 appeared semi-metallic. These apparently metallic subsamples were the only two to exhibit a superconducting response. To determine the superconducting phase within these apparently metallic subsamples, it was necessary to measure the elemental composition of all the subsamples and observe the differences.

Each of the subsamples measured in the divide and conquer process were measured using the Energy-Dispersive X-Ray Spectroscopy (EDX) detector on a scanning electron microscope (SEM). The EDX spectra for the subsamples from Mundrabilla (Fig. 2.4a) showed that the superconducting subsamples, A and C, contained lead, indium and tin. The non-superconducting subsample, B, did not contain lead, indium or tin. Similarly, the EDX spectra for the subsamples from GRA 95205 (Fig. 2.4b) showed that only the spectra from the superconducting subsamples (4 and 5) had significant indium and tin peaks. Subsample 1 showed very small indium and tin peaks while subsamples 2 and 3 did not show any evidence of indium or tin. None of the GRA 95205 samples showed a significant lead presence. This suggested that the superconducting phase within the samples was likely an alloy of lead, indium and tin in Mundrabilla and an alloy of indium and tin in GRA 95205

The multiple peaks observed in the MFMMS signal for the various subsamples in Figure 3 are consistent with this conclusion. Lead and lead alloys are superconducting at these temperatures (*18*). Indium and lead alloys have a range of critical temperatures, decreasing with increasing indium concentration (*19*). Indium and tin alloys have critical temperatures below 4 K

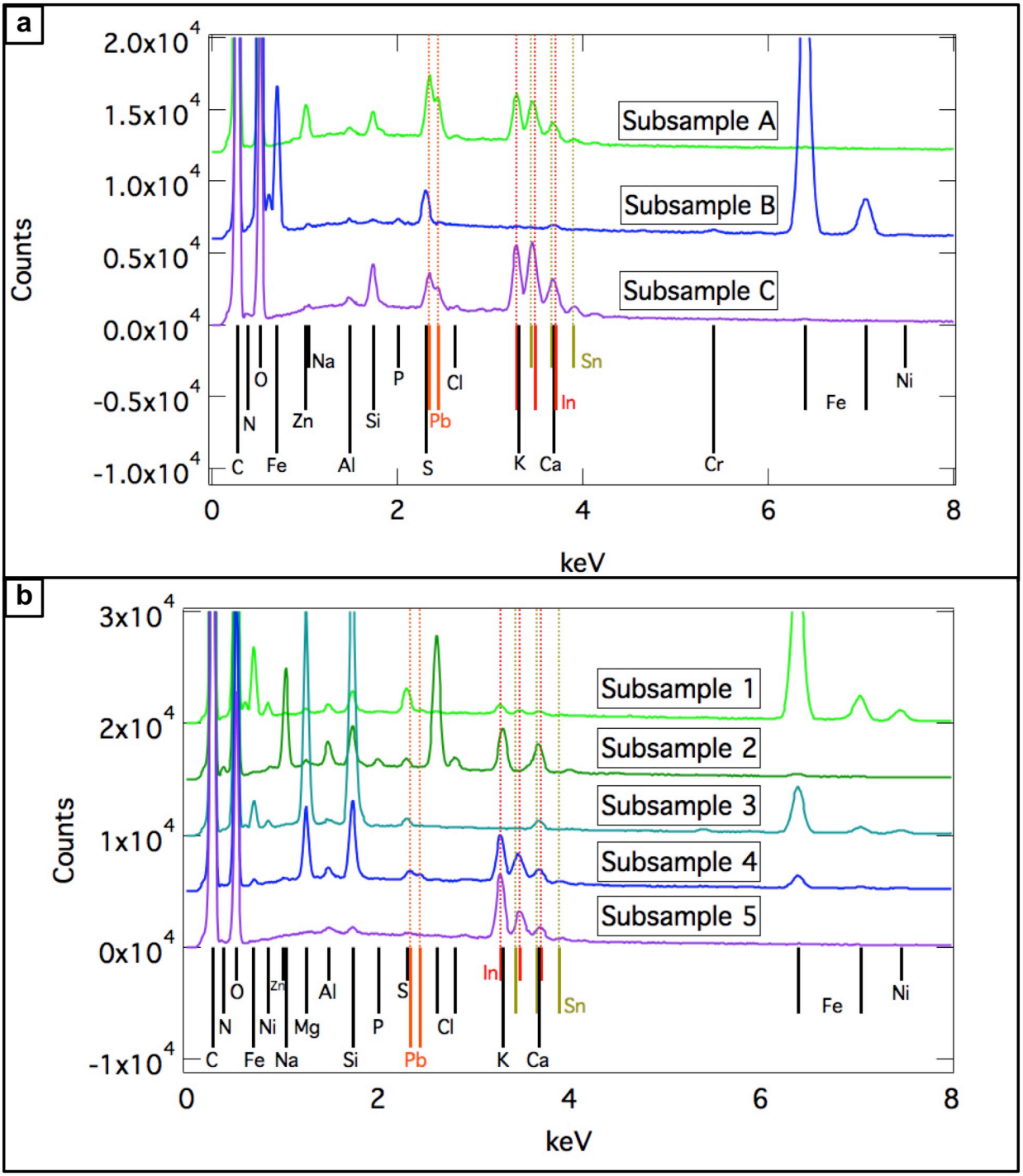

Figure 2.4: EDX data measured from grains taken from subsamples of (a) Mundrabilla and (b) GRA 95205. Measurements are normalized and vertically offset for clarity. Black lines show ideal energies for EDX peaks of elements. Pb, In and Sn have colored labels, to highlight them for visual clarity.

at high concentrations of either metal, but alloys with moderate concentrations of each have critical temperatures above 6 K (*20*). Therefore, multiple grains with varying ratios of metals would produce multiple superconducting critical temperatures.

Table 2.1: SUPERCON database analysis of subsamples. Cells show maximum volume percentage of a given superconducting phase that could be contained within a given subsample, assuming the EDX measurement of the subsample surface is representative of the whole. Each entry in SUPERCON is separately compared to the EDX measurements. This list is sorted by volume percentage and is a complete analysis of every entry in SUPERCON with a T_c between 5 K and 8 K. Some entries have been condensed into a single entry on this list, (ie: $In_{0.6}Pb_{0.4}$ and $In_{0.5}Pb_{0.5}$ are both listed as In_xPb_y) and the volume for these combined entries is that of the highest individual entry. Entries in the database that are superconducting only under pressure were excluded from the list.

Meteorite	**Mundrabilla**		
Subsample	**A**	**B**	**C**
1st vol. %	In_xPb_y - 38.31%	$Ca_xAl_ySi_z$ - 0.4572%	Pb_xSn_y - 33.89%
2nd vol. %	Pb_xSn_y - 35.04%		Pb - 13.70%
3rd vol. %	In_xSn_y - 25.49%		$Pb_{0.9}Zn_{0.1}$ - 11.92%
4th vol. %	$Pb_{0.9}Zn_{0.1}$ - 25.32%		
5th vol. %	Pb - 24.47%		
6th vol. %	Mg_xPb_y - 2.176%		
7th vol. %	$Mg_xAl_ySi_z$ - 0.09144%		
Meteorite	**GRA 95205**		
Subsample	**1**	**2**	**3**
1st vol. %	MgC_yNi_3 - 2.629%	C_2Na - 23.90%	$MgCNi_{3-z}Fe_z$ - 1.841%
2nd vol. %	$MgC_yNi_{3-z}Fe_z$ - 2.543%	$Ca_xAl_ySi_z$ - 5.296%	MgC_yNi_3 - 1.720%
3rd vol. %	In_xSn_y - 1.724%	NaAlSi - 3.906%	
4th vol. %	$Ca_xAl_ySi_z$ - 1.033%	$Mg_xAl_ySi_z$ - 1.316%	
5th vol. %	$Mg_xAl_ySi_z$ - 0.9503%		
Meteorite	**GRA 95205**		
Subsample	**4**	**5**	
1st vol. %	In_xSn_y - 22.95%	In_xPb_y - 7.324%	
2nd vol. %	In_xPb_y - 20.73%	$Ca_xAl_ySi_z$ - 2.465%	
3rd vol. %	Pb_xSn_y - 10.84%	CaPb - 2.111%	
4th vol. %	Cu_xSn_y - 6.842%	$Cu_{0.1}Pb_{0.9}$ - 1.829%	
5th vol. %	Mg_xPb_y - 6.182%	Mg_xPb_y - 1.792%	
6th vol. %	$Cu_{0.1}Pb_{0.9}$ - 5.178%	Pb - 1.769%	
7th vol. %	Pb - 5.007%		
8th vol. %	$Mg_xAl_ySi_z$ - 4.597%		
9th vol. %	$MgC_yNi_{3-z}Fe_z$ - 0.9131%		
10th vol. %	$Mg_xC_yNi_3$ - 0.8719%		
11th vol. %	$MgC_yNi_{3-z}Cu_z$ - 0.8523%		

To support this explanation, we created an algorithm to compare each set of EDX data with every superconducting phase in the SUPERCON database (*21*) with T_c between 5 K and 8 K. This method created a list of every superconducting candidate in the SUPERCON database, for each subsample from Mundrabilla and GRA 95205 based on the elements detected using EDX. These lists were sorted by the maximum volume percentage that each superconducting candidate could have in the sample, based on the availability of elements in the meteorite subsamples (Table 2.1). This analysis assumes the EDX analysis was representative of the bulk content. The calculation showed that out of all superconductors in SUPERCON, those with the

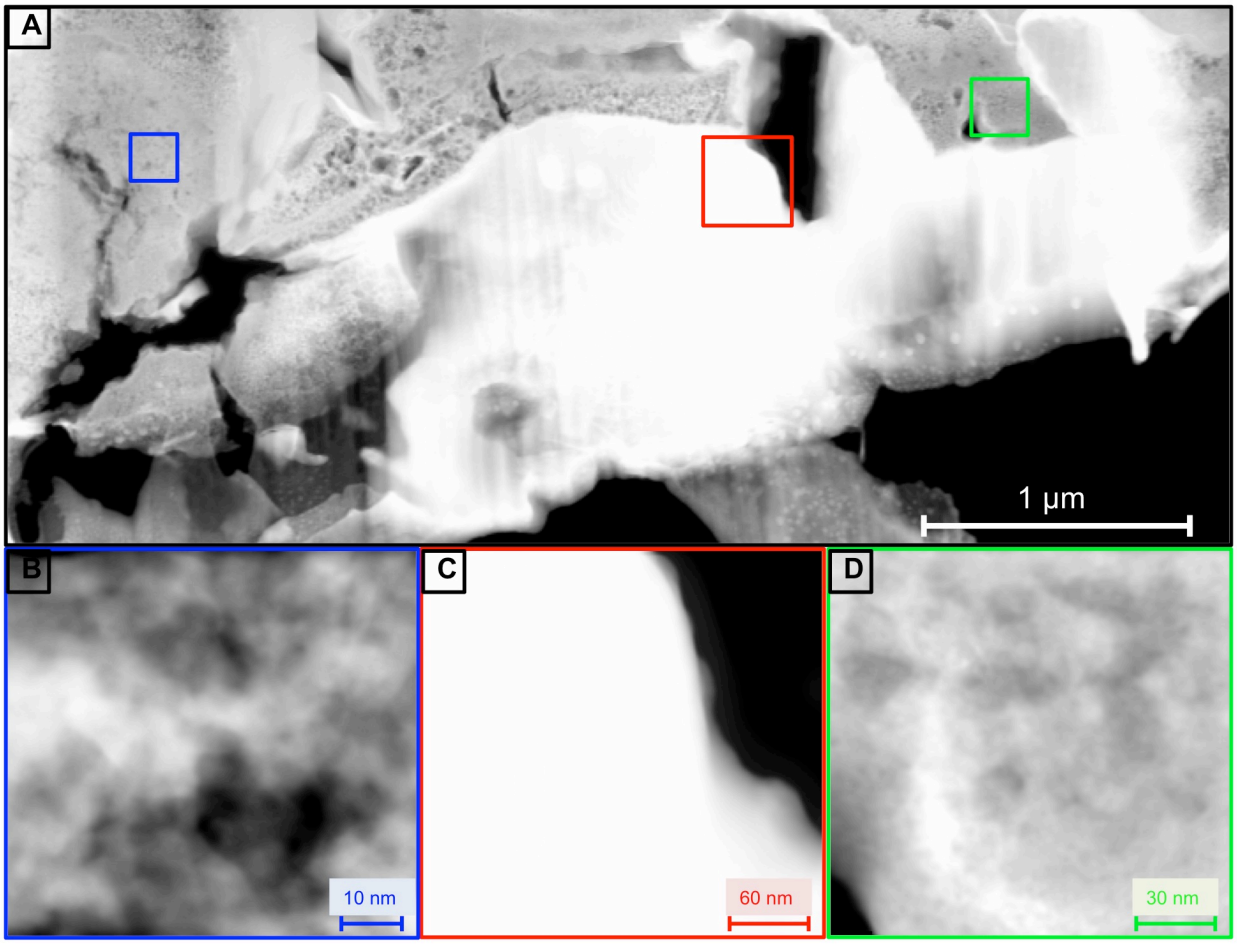

Figure 2.5: TEM images of superconducting Mundrabilla Sample. TEM images of grain from Mundrabilla subsample A. Shown are a larger image (A) and smaller images. Blue (B), red (C) and green (D) colored outlines in larger image correspond to imaged areas (B-D).

highest possible volume percentage in the superconducting subsamples were alloys of indium, tin and lead.

Table 2.2: TEM EDX measurements of superconducting Mundrabilla sample. Weight percentage and atomic percentage breakdown of elements from TEM EDX measurements of different sections of a grain from a superconducting sample of Mundrabilla. TEM image of the respective sections is shown in Fig. 2.5. Errors presented are 1 sigma.

Element	**Fig. 2.5b**		**Fig. 2.5c**		**Fig. 2.5d**	
	Weight %	**Atomic %**	**Weight %**	**Atomic %**	**Weight %**	**Atomic %**
In	74.7±10.0	75.3±10.1	76.1±10.2	78.7±10.5	76.9±11.0	67.9±9.7
Sn	15.4±3.6	15.0±3.5	11.2±3.0	11.2±3.0	12.4±3.6	10.6±3.0
Pb	8.75±3.24	4.89±1.81	11.89±3.80	6.81±2.18	5.79±2.98	2.83±1.45
Mg					0.46±0.35	1.91±1.45
Si	1.17±0.50	4.81±2.06	0.77±0.41	3.25±1.73	1.54±0.65	5.57±2.36
Al					2.99±0.89	11.24±3.36
Total	100.00	100.00	100.00	100.00	100.00	99.99

To verify this, a state-of-the-art Super EDX detector on a Transmission Electron Microscope (TEM) was used to measure one of the superconducting grains from Mundrabilla subsample A. The surface layers of the sample were removed with Focused Ion Beam (FIB) and TEM images were taken of the interior (Fig. 2.5.), along with EDX analysis of nanoscale regions of the sample (Table 2.2). All of the regions imaged were predominantly indium, lead and tin, with indium making up the majority of each region. Trace quantities of aluminum, silicon and magnesium were also present in some regions. Because alloys of lead indium and tin have been shown to be superconducting at these temperatures and these elements are present with high purity in the grains that are superconducting, these alloys are likely the phases responsible for the MFMMS response.

2.3 Discussion

Superconductivity in natural samples (ie: those formed by natural processes, without further treatment) is extremely unusual. Naturally collected minerals are not phase-pure materials

(*22*). Even the simplest superconducting mineral, lead, is only rarely found naturally in its native form and to our knowledge, there are no previous reports of natural lead samples superconducting (though it is still possible that sufficiently pure natural lead exists). In fact, we are only aware of one previous report of superconductivity in natural materials, in the mineral covellite, with a T_c of 1.6 K (*22*). However, the superconducting phases reported here likely exist in other meteorites, since such similar phases have been found in two dissimilar meteorites. This assumption is consistent with the abundance of these elements in other meteorites and the solar system at large. Lead and tin have moderate abundance, whereas indium is another order of magnitude less abundant, but still more abundant than the rare earths (*1*). Within ureilites, irons, and other meteorites, their abundances vary significantly (*23*, *24*).

While these nonchondritic meteorites do not carry a history of the interstellar medium (*1*), the fact that these phases can form naturally in macroscopic grains shows that there exists a natural process that can create these phases. This suggests the possibility that superconducting material phases could also be found in interstellar grains deep within the coldest regions of space, where these phases would be in a superconducting state. For example, cold dense molecular clouds have typical temperatures as low as 10 K (*25*), but in regions with particularly low ultraviolet stellar radiation, temperatures are estimated to be as low as 5 K (*26*). In unusual parts of space, temperatures can be even lower (*27*). The superconducting phases detected in these meteorites would be superconducting in these regions. Furthermore, other metallic alloys have been shown to have critical temperatures above 10 K (*28*, *29*), which could exist naturally if they could be created in similar conditions to the phases detected in this manuscript.

Superconducting particles within cold regions of space could have implications on the structure of stellar objects. Specifically, superconducting particles could sustain microscopic

current loops generated by transient fields and contribute to nearby magnetic fields. The origins of some magnetic fields, such as those observed in giant molecular clouds (*30*) are not well understood. Whether or not naturally superconducting phases would have any significant effect would depend on the critical temperature and quantity of such phases, and therefore deserves further study. There is an aggressive expansion of research and new missions to space, searching for new materials in extraterrestrial objects. This study suggests that the search for naturally occurring superconducting grains and their roles in astronomical objects should be a new component of such research. (*31*)

2.4 Methods

2.4.1 Meteorite Selection Criteria

A diverse population of meteorites was measured (Table 2.3). Among chondrites, a range of chemical groups and petrologic types were measured. Among nonchondrites, primitive achondrites (including GRA 95205, a ureilite), magmatic achondrites (a eucrite, a diogenite and an aubrite) and two different irons (including Mundrabilla) were measured. In previous studies, we have also studied micrometeorites (*16*), martian meteorites and lunar rocks. Initially, meteorites with extreme formation conditions in their history were selected to measure (including both Mundrabilla and GRA 95205), although others were later added to represent other classes of meteorites. While no meteorite is fully representative of the range of interesting chemical phases within any given class of meteorites, this set of meteorites provided a good representative sample that spans the classes of meteorites (*1*).

Table 2.3: List of meteorites measured with MFMMS. Samples from each of the following meteorites were measured. A "yes" in the third column indicates that one or more samples scraped from the meteorite was superconducting.

Meteorite Name	Type	Superconducting
Mundrabilla	Iron IAB	**Yes**
GRA 95205	Ureilite	**Yes**
ALHA77216.85	Ordinary Chondrite (L)	No
LAP 91900	Diogenite	No
Abee	Enstatite Chondrite	No
PCA 82502	Eucrite	No
EET 97511	Ureilite	No
North County	Aubrite	No
PCA 91241	Rumuruti Chondrite R3.8-6	No
ALHA 81021	Enstatite Chondrite EL6	No
EET 83213	Ordinary Chondrite LL3.7	No
Santa Clara	Iron IVB	No
Allende	Carbonaceous Chondrite CV3	No
LEW 85311	CM Carbonaceous Chondrite (Anomalous)	No
Murchison	Carbonaceous Chondrite CM2	No

2.4.2 MFMMS

Samples were prepared by first scraping meteorites to dislodge powder from the bulk of the meteorite sample. Powder was inserted into quartz tubes for use in MFMMS. The quartz tubes were then flushed with helium and sealed. MFMMS measurements were performed with a variable DC Field, H_{DC}, and an AC Field, H_{AC}, of 15 Oe, applied parallel to the microwave magnetic field, as described previously (*8*). Measurements with sequences of DC fields applied (Fig. 2.1, 2.3) are applied in strictly increasing sequences.

2.4.3 VSM

Samples were measured in the Quantum Design PPMS Dynacool VSM option. Each sample that was measured in the VSM had previously been screened in MFMMS. In order to recover the powder from a MFMMS tube, the tube was broken and the powder was scraped out

of the end of the tube in a clean environment. The resultant sample was then inserted into the VSM.

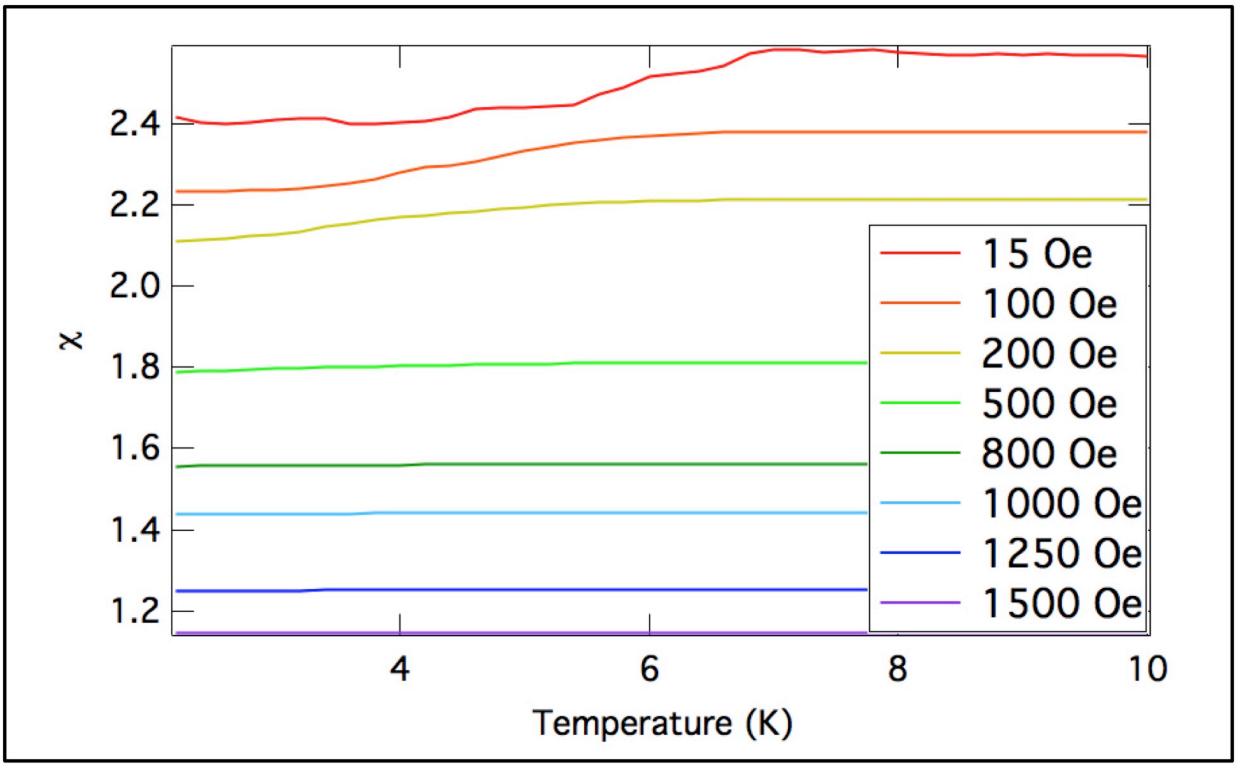

Figure 2.6: VSM measurements of Mundrabilla without data offset. VSM measurements of samples from Mundrabilla. ZFC measurements on sample MUND-1 were performed with applied magnetic field ranging from 15-1500 Oe. Data is not vertically offset.

ZFC measurements of samples were performed by cooling without any applied magnetic field and then applying a field before measurement. FC measurements were performed at the same fields by applying a magnetic field and then measuring while heating. At 5 Oe and 10 Oe (Fig. 2.2c), five separate averages at each temperature point were taken consecutively, to account for the increased noise at these fields. For clarity, data in the images was offset from Fig. 2.6. In VSM measurements of sample MUND-2 (Fig. 2.2d), data was collected while temperature was sweeping – made possible by the increased signal in that sample.

VSM measurements were performed on samples from Mundrabilla due to the strength of the superconducting response in MFMMS and the larger number of superconducting samples found.

2.4.4 Sample Volume Measurements

VSM measurements give the magnetic moment of a sample. To calculate the average magnetization within a sample, it was necessary to determine the sample volume, which was difficult to do precisely. The two easiest methods that might be used were measuring volume by liquid displacement, and measuring the mass and converting to volume using a known density.

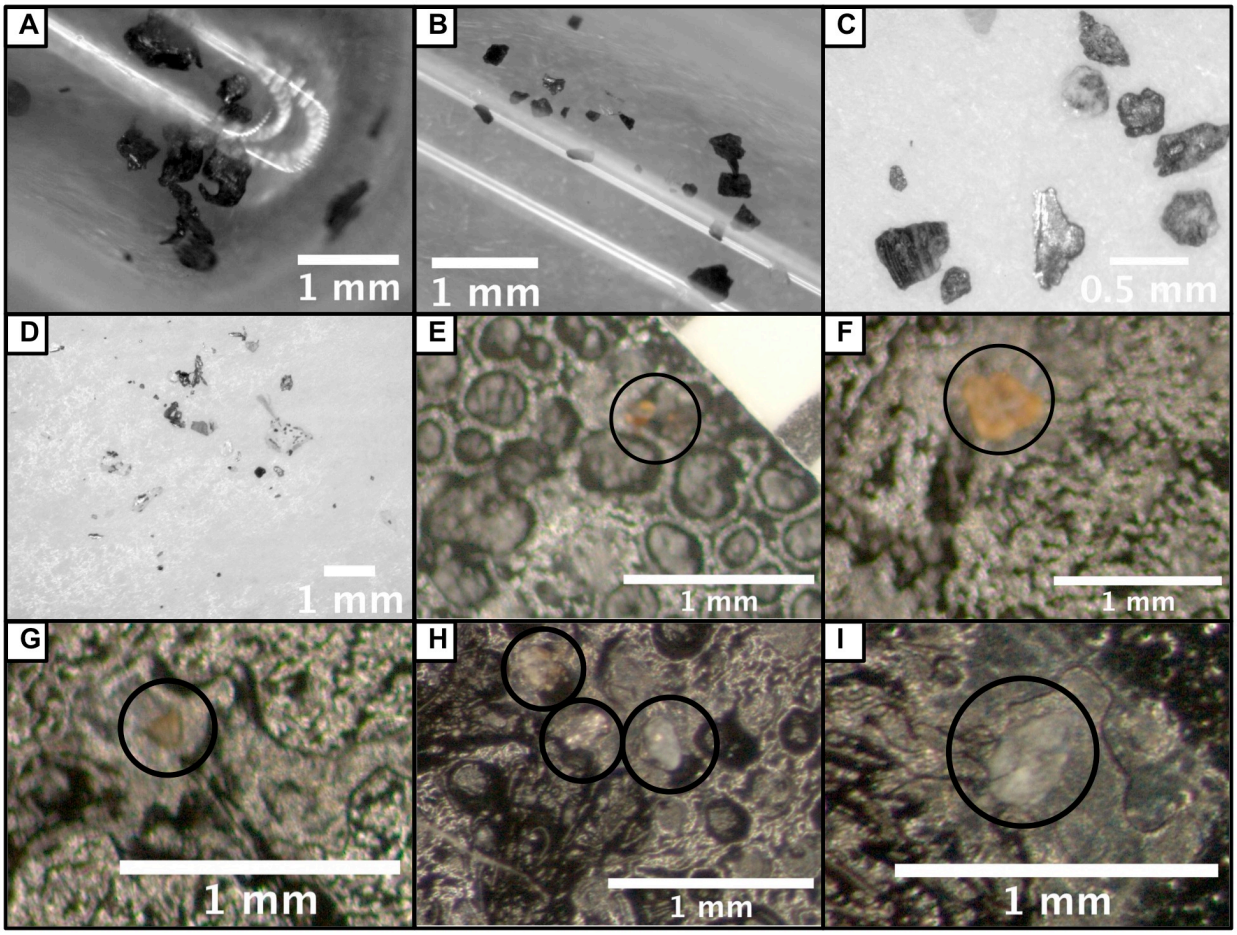

Figure 2.7: Images of Meteorite samples and subsamples. Images of MUND-2 subsamples A (a), B (b) and C (c) are shown. Subsamples A and B are imaged inside of quartz tube. Image of MUND-1 (d) is shown. Images of GRA-1 subsamples 1 (e), 2 (f), 3 (g), 4 (h) and 5 (i) are shown on a carbon tape background.

The sample volumes were too small for most liquid displacement techniques, with sample volumes below 1 mm^2 (1 microliter displacement). And the density could not be easily determined: not only are these samples natural materials, but the methods described in this paper select out specific samples from the larger bulk, adding a strong selection bias.

Previous studies on micrometeorites have attempted to estimate volumes of samples with similar size scales as the grains measured in this paper by making inferences from 2D images. One study estimated volumes of approximately spherical samples by taking 2D images and assuming equal semiminor axes (*32*). Other studies estimate volume by imaging samples, outlining them, and then using a configuration with a low depth of focus to measure height (*33*, *34*). However, the grains studied in this work are not approximately spherical (Fig. 2.7) and the height of the particles is insufficiently regular for the latter method. In order to come up with a volume estimate, we combined these two approaches, outlining the samples, and measuring a property termed the "local thickness" of each pixel in each grain to calculate an average in-plane thickness.

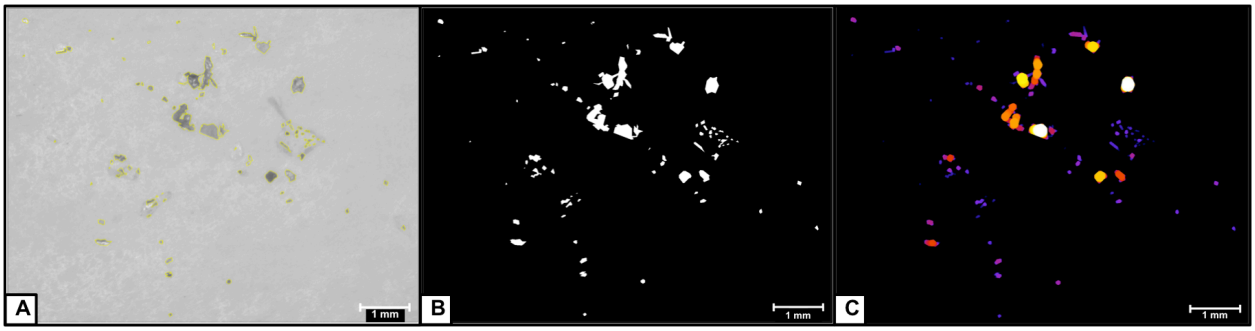

Figure 2.8: Method: segmentation and calculation of local thickness. Images produced in ImageJ software for calculation of local thickness. Sample MUND-1 imaged with an optical microscope and outlined in yellow using ImageJ software (a). Mask created of previous image (b). Local thickness calculation based on mask (c) with bright areas indicating large local thickness and dim areas indicating small local thickness.

In order to determine the volume of the samples, the samples were imaged with an optical microscope and camera. ImageJ software (*35*) was used to outline and calculate the area of the

samples (Fig. 2.8a, 2.8b). Using this outline, the local thickness was calculated (*36*) (Fig. 2.8c). Local thickness is defined as the diameter of the largest circle that could fit within the sample at each point. The out of plane thickness of the sample can then be roughly estimated by calculating the average local thickness. Note that this is not a direct measurement of the out of plane thickness, but simply an estimate based on the assumption that these samples are either approximately regular or approximately randomly oriented.

Table 2.4: Volume estimate of Mundrabilla samples. Volume estimate and related values for samples and subsamples from Mundrabilla. ETMUND-2 is the sum of subsamples A, B and C and volume was calculated by added together the preceding subsamples.

	Volume (cm^3)	**Error (cm^3)**	**Area (cm^2)**	**Local Thickness (cm)**	**Local Thickness Error (cm)**
ETMUND-1	9.10×10^{-5}	7.99×10^{-5}	9.80×10^{-3}	9.29×10^{-3}	5.35×10^{-3}
ETMUND-2	8.06×10^{-4}	5.40×10^{-4}			
Subsample A	5.11×10^{-4}	3.51×10^{-4}	1.58×10^{-2}	3.24×10^{-2}	1.25×10^{-2}
Subsample B	9.37×10^{-5}	6.88×10^{-5}	5.28×10^{-3}	1.77×10^{-2}	7.54×10^{-3}
Subsample C	2.01×10^{-4}	1.20×10^{-4}	7.91×10^{-3}	2.54×10^{-2}	7.45×10^{-3}

To quantify the error contribution of that assumption, multiple measurements were taken of very irregular grains from sample MUND-2, subsample A. These grains were placed inside a quartz tube and pictures were taken while the tube was rotated. The variance of this measurement gave an upper bound on this contribution to uncertainty, of 29.88% of a given sample's volume. The total error for a given volume estimate is calculated from that contribution, an approximate error of 0.05 mm^2 from outlining the samples, and the standard deviation in the local thickness for a particular volume estimate. Using this method, the volume and uncertainty of samples could be estimated (Table 2.4).

2.4.5 Divide and Conquer

The Divide and Conquer process involved dividing samples into subsamples, in order to determine what grains within a sample contained superconductivity. In order to do this, samples were examined with an optical microscope and completely separated based on their visual

morphology (a subjective assessment based on the appearance of individual grains) into different subsamples. This initial step was qualitative and the success or failure of it was determined by subsequent measurements. To do this, the subsamples were individually measured in MFMMS to determine which subsamples produced a superconducting response and how strong that response was. If some of the subsamples were not superconducting, they could be analyzed and compared with the superconducting ones, to determine what the superconducting phase was.

2.4.6 Scanning Electron Microscopy (SEM) EDX

Individual grains were selected from the subsamples resulting from the divide and conquer process and placed on carbon tape. These grains were then measured in an FEI Quanta 250 SEM using the EDX option. Multiple locations were measured in order to ensure that the surface was sufficiently homogenous. By examining the difference between superconducting and non-superconducting grains, it was possible to determine what elements were unique to the superconducting grains. By comparing these elements to the chemical makeup of known superconductors with critical temperatures near those measured in MFMMS, it was possible to determine the likely superconducting compound.

2.4.7 SUPERCON

Table 2.5: EDX measurements of Mundrabilla subsamples. Weight percentage and atomic percentage breakdown of elements from EDX measurements of Mundrabilla subsamples. Errors presented are 1 sigma.

Element	Subsample A		Subsample B		Subsample C	
	Weight %	Atomic %	Weight %	Atomic %	Weight %	Atomic %
O	38.721±0.171	82.171±0.363	44.501±0.125	73.065±0.206	43.401±0.248	80.070±0.458
Mg	0.028±0.033	0.039±0.045				
Al	0.557±0.052	0.701±0.066	0.202±0.014	0.196±0.014	0.509±0.051	0.557±0.056
Si	1.500±0.045	1.815±0.055	0.168±0.007	0.157±0.007	3.103±0.050	3.262±0.052
P			0.179±0.016	0.152±0.013		
S			1.481±0.017	1.214±0.014		
Cl			0.075±0.007	0.056±0.005	0.319±0.028	0.265±0.024
K			0.061±0.006	0.041±0.004	7.875±0.096	5.945±0.073
Ca			0.156±0.014	0.102±0.009		
Cr			0.303±0.017	0.153±0.008		
Fe	0.490±0.041	0.298±0.025	52.620±0.105	24.751±0.050	0.482±0.044	0.255±0.023
Ni			0.254±0.040	0.113±0.018		
Zn	3.890±0.163	2.022±0.085			0.404±0.075	0.182±0.034
In	17.390±0.300	5.147±0.089				
Sn	12.957±0.345	3.710±0.099			30.205±0.167	7.512±0.042
Pb	24.466±0.985	4.013±0.162			13.701±1.014	1.952±0.145
Total	99.999	100.000	100.000	100.000	99.999	100.000

In order to support the previous determination, the SEM-EDX data (Tables 2.5, 2.6) was analyzed using information from the SUPERCON database (*21*). An algorithm was written that compared each superconducting entry in SUPERCON with T_c between 5 K and 8 K at ambient pressure to each set of EDX data (Fig. 2.4). These superconducting entries were sorted by the maximum possible volume percentage the phase could have within a given sample, assuming the EDX data was characteristic of the bulk of the sample. This data was sorted by this maximum volume percentage (Table 2.1).

Table 2.6: EDX measurements of GRA 95205 subsamples. Weight percentage and atomic percentage breakdown of elements from EDX measurements of GRA 95205 subsamples. Errors presented are 1 sigma.

Element	Subsample 1		Subsample 2		Subsample 3	
	Weight %	Atomic %	Weight %	Atomic %	Weight %	Atomic %
O	36.955±0.105	66.517±0.188	61.031±0.236	74.839±0.290	41.112±0.117	55.459±0.158
F					10.861±0.061	12.338±0.070
Na			11.689±0.093	9.976±0.080		
Mg	0.291±0.018	0.345±0.021	0.403±0.035	0.326±0.028	13.911±0.054	12.353±0.048
Al	0.537±0.018	0.573±0.019	1.350±0.053	0.982±0.039		
Si	1.093±0.015	1.121±0.016	2.414±0.047	1.687±0.033	16.613±0.037	12.767±0.029
P	0.094±0.007	0.088±0.007	0.619±0.022	0.392±0.014		
S	1.676±0.014	1.506±0.013	0.957±0.045	0.586±0.028	0.582±0.014	0.392±0.009
Cl	0.074±0.006	0.060±0.005	11.995±0.068	6.638±0.038	0.080±0.007	0.049±0.004
K			4.698±0.060	2.357±0.030		
Ca	0.302±0.008	0.217±0.006	3.681±0.064	1.802±0.031	0.952±0.015	0.513±0.008
Ti			0.145±0.028	0.059±0.011		
Cr	0.144±0.009	0.080±0.005			0.484±0.020	0.201±0.008
Mn					0.181±0.028	0.071±0.011
Fe	51.578±0.096	26.597±0.050	1.016±0.086	0.357±0.030	13.845±0.051	5.351±0.020
Ni	4.226±0.048	2.073±0.023			1.379±0.039	0.507±0.014
Cu						
Zn	0.346±0.027	0.152±0.012				
In	2.471±0.058	0.620±0.014				
Sn	0.213±0.029	0.052±0.007				
I						
Pb						
Total	100.000	100.000	99.998	100.000	100.000	100.000

Table 2.6: EDX measurements of GRA 95205 subsamples. Weight percentage and atomic percentage breakdown of elements from EDX measurements of GRA 95205 subsamples. Errors presented are 1 sigma (continued).

Element	Subsample 4		Subsample 5	
	Weight %	Atomic %	Weight %	Atomic %
O	55.134±0.158	82.494±0.236	57.412±0.235	88.710±0.363
F				
Na				
Mg	4.801±0.028	4.729±0.027	0.157±0.020	0.159±0.021
Al	0.595±0.026	0.528±0.023	0.699±0.032	0.640±0.029
Si	5.084±0.021	4.334±0.018	0.764±0.027	0.672±0.024
P				
S			0.240±0.016	0.185±0.012
Cl	0.181±0.022	0.122±0.015	0.214±0.015	0.149±0.010
K				
Ca			1.932±0.062	1.192±0.039
Ti				
Cr	0.151±0.012	0.069±0.006		
Mn	0.072±0.016	0.032±0.007		
Fe	3.592±0.040	1.540±0.017	0.371±0.029	0.164±0.013
Ni	0.684±0.044	0.279±0.018		
Cu	0.396±0.051	0.149±0.019	0.621±0.084	0.242±0.033
Zn	0.779±0.064	0.285±0.023		
In	17.065±0.119	3.558±0.025	33.993±0.165	7.319±0.040
Sn	6.458±0.135	1.303±0.027		
I			1.828±0.207	0.356±0.040
Pb	5.007±0.218	0.578±0.025	1.769±0.330	0.211±0.039
Total	100.000	100.000	100.000	100.000

Specifically, the code performed the following steps on each EDX dataset:

1. Reads in all information from SUPERCON and EDX dataset
2. EDX reports concentrations in mass percentage of the whole sample.
3. Compares each compound in SUPERCON to the EDX dataset:
    a. Determine the total molecular mass of the compound
    b. For each element, calculate $Mm_e/a_e n_e$, where M is the total molecular mass of the compound, m_e is the mass fraction of the element in the EDX dataset, a_e is the

atomic mass of the element and n_e is the number of the element in the chemical formula of the compound.

i. This gives the total possible weight fraction of the superconducting compound within the sample, based only one how much of that one element is available.

c. Determine this number for each element in superconducting compound.

d. The lowest of these numbers is total possible weight fraction of the superconducting compound within the sample.

e. Convert weight fraction to weight percent

f. Note that carbon and oxygen are ignored for these calculation due to the carbon tape background and potentially oxidized surface (which would not necessarily be representative of the interior).

4. Removes all superconducting compounds with T_c below 5 K or above 8 K or compounds of only carbon and oxygen.

5. Sorts the remaining superconducting compounds by the aforementioned possible weight percent

Compounds that were superconducting only under pressure were removed manually after the code ran. The code is available from the corresponding author upon reasonable request.

2.4.8 Transmission Electron Microscopy

Due to the large number of superconducting samples available, TEM measurements were performed on samples from the Mundrabilla meteorite. The samples were made by standard lift-out method by an FEI Helios dual beam system. The samples were further trimmed at low voltage mode to remove the surface amorphous layers. Elemental mappings were conducted on a

high-resolution analytical transmission electron microscope (TEM, FEI Talos F200X) operating at 200 kV. The elemental mappings were acquired with a four-quadrant 0.9 sr energy dispersive X-ray spectrometer (Super EDX).

2.5 Acknowledgements

Chapter 2 was prepared based on material submitted for publication: Wampler, James; Thiemens, Mark; Cheng, Shaobo; Zhu, Yimei; Schuller, Ivan K. "Natural Superconductivity Found in Meteorites." J.W. performed the experiments, M.T. provided the meteorites and I.K.S. supervised the project. S.C. conducted the TEM experiments under the supervision of Y. Z.. All authors contributed to the data analysis and writing of the manuscript. J. W. was the principal researcher/author on this paper.

We thank Ilya Valmianski for help with SEM-EDX measurements, Alex Hojem for help editing the manuscript and James Day for taking complementary measurements of the meteorites reported on in this paper. Harold Weinstock's original suggestion for the search for superconductivity in extraterrestrial materials is gratefully acknowledged. **Funding:** supported by the Air Force Office of Scientific Research (grant FA9550-14-1-0202); transmission electron microscopy work at BNL was supported by the U.S. Department of Energy, Office of Basic Energy Science, Division of Materials Science and Engineering, under Contract No. DE-SC0012704.

2.6 References

1. H. Y. J. McSween, G. R. Huss, *Cosmochemistry* (University Press, Cambridge, 2010).
2. J. Fritz, A. Greshake, V. A. Fernandes, Revising the shock classification of meteorites. *Meteorit. Planet. Sci.* **52**, 1216 (2017).
3. J. I. Goldstein, E. R. D. Scott, N. L. Chabot, Iron meteorites: Crystallization, thermal history, parent bodies, and origin. *Chemie der Erde*. **69**, 293 (2009).
4. L. Bindi, C. Lin, C. Ma, P. J. Steinhardt, Collisions in outer space produced an icosahedral

phase in the Khatyrka meteorite never observed previously in the laboratory. *Sci. Rep.* **6**, 10 (2016).

5. P. H. Warren, J. T. Wasson, The origin of KREEP. *Rev. Geophys.* **17**, 73 (1979).

6. L. W. Alvarez, W. Alvarez, F. Asaro, H. V. Michel, Extraterrestrial Cause for the Cretaceous-Tertiary Extinction. *Science*. **208**, 1095 (1980).

7. D. S. Burnett, NASA returns rocks from a comet. *Science*. **314**, 1709 (2006).

8. J. G. Ramírez, A. C. Basaran, J. de la Venta, J. Pereiro, I. K. Schuller, Magnetic field modulated microwave spectroscopy across phase transitions and the search for new superconductors. *Reports Prog. Phys.* **77**, 093902 (2014).

9. I. Goldstein, B. Halpern, L. Robert, The Mundrabilla Meteorite: a New Discovery in Western Australia. *Nature*. **213**, 274 (1967).

10. J. N. Grossman, The Meteoritical Bulletin, No. 82, 1998 July. *Meteorit. Planet. Sci.* **33**, A221 (1998).

11. J. T. Wasson, G. W. Kallemeyn, The IAB iron-meteorite complex: A group, five subgroups, numerous grouplets, closely related, mainly formed by crystal segregation in rapidly cooling melts. *Geochim. Cosmochim. Acta*. **66**, 2445 (2002).

12. E. R. D. Scott, Origin of rapidly solidified metal-troilite grains in chondrites and iron meteorites. *Geochim. Cosmochim. Acta*. **46**, 813 (1982).

13. A. E. Rubin, Shock, post-shock annealing, and post-annealing shock in ureilites. *Meteorit. Planet. Sci.* **41**, 125 (2006).

14. J. de la Venta, A. C. Basaran, T. Grant, A. J. S. Machado, M. R. Suchomel, R. T. Weber, Z. Fisk, I. K. Schuller, Methodology and search for superconductivity in the La–Si–C system. *Supercond. Sci. Technol.* **24**, 075017 (2011).

15. T. Saerbeck, J. Pereiro, J. Wampler, J. Stanley, J. Wingert, O. G. Shpyrko, I. K. Schuller, Ferromagnetism in partially oxidized CuCl. *J. Magn. Magn. Mater.* **346**, 161 (2013).

16. S. Guénon, J. G. Ramírez, A. C. Basaran, J. Wampler, M. Thiemens, S. Taylor, I. K. Schuller, Search for superconductivity in micrometeorites. *Sci. Rep.* **4**, 7333 (2014).

17. S. Guénon, J. G. Ramírez, A. C. Basaran, J. Wampler, M. Thiemens, I. K. Schuller, Search for New Superconductors: an Electro-Magnetic Phase Transition in an Iron Meteorite Inclusion at 117 K. *J. Supercond. Nov. Magn.* **30**, 297 (2017).

18. B. Damaschke, R. Tidecks, V. H. Teichler, The superconducting transition temperatures of some dilute lead alloys. *Proc. Phys. Soc.* **86**, 1199 (1965).

19. D. K. Farrell, B. S. Chandrasekhar, Properties of Superconducting Lead-Indium Alloys

and the Generalized Ginzburg-Landau Parameter κ_2. *Phys. Rev.* **216**, 401 (1969).

20. M. F. Merriam, M. Von Herzen, Superconductivity in the indium-tin system. *Phys. Rev.* **131**, 637 (1963).

21. Superconducting Material Database (SuperCon). *Natl. Inst. Mater. Sci.* (2011), (available at https://supercon.nims.go.jp/index_en.html).

22. F. Di Benedetto, M. Borgheresi, A. Caneschi, G. Chastanet, C. Cipriani, D. Gatteschi, G. Pratesi, M. Romanelli, R. Sessoli, First evidence of natural superconductivity: covellite. *Eur. J. Mineral.* **18**, 283 (2006).

23. P. A. Baedeker, P. R. Buseck, V. M. Oversby, *Handbook of Elemental Abundances in Meteorites* (Gordon and Breach Science Publishers, New York, 1971).

24. P. H. Warren, F. Ulff-Møller, H. Huber, G. W. Kallemeyn, Siderophile geochemistry of ureilites: A record of early stages of planetesimal core formation. *Geochim. Cosmochim. Acta*. **70**, 2104 (2006).

25. E. A. Bergin, M. Tafalla, Cold Dark Clouds: The Initial Conditions for Star Formation. *Annu. Rev. Astron. Astrophys.* **45**, 339 (2007).

26. J. M. Greenberg, Interstellar Grain Temperatures. Effects of Grain Materials and Radiation Fields. *Astron. Astrophys.* **12**, 240 (1971).

27. R. Sahai, L.-Å. Nyman, The Boomerang Nebula: The Coldest Region of the Universe? *Astrophys. J.* **487**, L155 (1997).

28. D. Dew-Hughes, Superconducting A-15 compounds : A review. *Cryogenics (Guildf).* **8**, 435 (1975).

29. J. Nagamatsu, N. Nakagawa, T. Muranaka, Y. Zenitani, J. Akimitsu, Superconductivity at 39 K in Magnesium Diboride. *Nature*. **410**, 63 (2001).

30. R. M. Crutcher, Magnetic Fields in Molecular Clouds. *Annu. Rev. Astron. Astrophys.* **50**, 29 (2012).

31. D. Shaltiel, H. Bill, A. Grayevsky, A. Junod, D. Lovy, W. Sadowski, E. Walker, Microwave Absorption across T_c: Determination of the angular dependance $H_{c2}(\theta)/H_{c2}$. *Phys. Rev. B*. **43**, 594 (1991).

32. C. Suavet, J. Gattacceca, P. Rochette, N. Perchiazzi, L. Folco, J. Duprat, R. P. Harvey, Magnetic properties of micrometeorites. *J. Geophys. Res. Solid Earth*. **114**, 1 (2009).

33. G. J. Flynn, S. R. Sutton, Cosmic Dust Particle Densities: Evidence for Two Populations of Stony Micrometeorites. *Proc. Lunar Planet. Sci.* **21**, 541 (1991).

34. S. G. Love, D. J. Joswiak, D. E. Brownlee, Densities of Stratospheric Micrometeorites.

Icarus. **111**, 227 (1994).

35. C. A. Schneider, W. S. Rasband, K. W. Eliceiri, NIH Image to ImageJ: 25 years of image analysis. *Nat. Methods*. **9**, 671 (2012).

36. R. Dougherty, K.-H. Kunzelmann, Computing Local Thickness of 3D Structures with ImageJ. *Microsc. Microanal.* **13**, 1678 (2008).

Chapter 3 – The Electromagnetic Origin of the Microwave Absorption Response of Fe_3O_4 Thin Films

3.1 Abstract:

Low field microwave absorption (LMFA) techniques are ultrasensitive, nondestructive methods of probing the electric and magnetic properties of a sample. Non-resonant LMFA techniques such as Magnetic Field Modulated Microwave Spectroscopy (MFMMS) can easily detect electromagnetic phase transitions in minute and inhomogeneous samples. However, while this technique can easily identify superconducting transitions, magnetic phase transitions produce more varied responses. This means that although these techniques are useful for the initial measurement of unknown samples, it is difficult to characterize an unknown magnetic sample or identify an unknown magnetic phase within a larger sample. Here, we present a technique to thoroughly investigate the electric and magnetic properties of a sample with a complex electromagnetic response. This technique involves taking a series of magnetic hysteresis loops and magnetoresistance measurements. These can be compared to MFMMS data to identify features as having an electric or magnetic origin. Magnetite (Fe_3O_4) possesses an electric, magnetic and structural phase transition across its Verwey transition. By measuring high quality Fe_3O_4 thin films in MFMMS and complementary techniques, the MFMMS signal is analyzed. Furthermore, a MFMMS signal can be calculated from the magnetic and electric data, which reproduces most of the features of the MFMMS signal.

3.2 Introduction:

Magnetic Field Modulated Microwave Spectroscopy (MFMMS) is a fast, ultrasensitive technique, adapted from older LFMA techniques (*1*, *2*). These techniques have primarily been used in the detection and characterization of superconductors (*3*, *4*), but some research has

focused on other materials (*5*–*7*) including bulk Fe_3O_4 (magnetite) (*8*). Although there has been some research on non-superconducting materials, the response of non-superconducting phase transitions in the MFMMS is not well understood. Superconducting transitions in the MFMMS consistently produce a characteristic peak signal. However, there is substantial variation in the response that magnetic transitions produce in the MFMMS (ie: different ferromagnetic transitions do not necessarily produce the same response). Without understanding why these responses differ, it is difficult to draw conclusions from the MFMMS signal of magnetic samples. For example, ferromagnetic transitions have been shown to have peaks in the MFMMS signal, dips, and step transitions (*4*).

Previous studies on the Verwey transition in Fe_3O_4 (magnetite) (*9*) have found changes in the MFMMS response across the transition (*8*, *10*). However, since the Verwey transition is a magnetic, resistive and structural transition, it is difficult to determine the physical origins of the features observed in the MFMMS response. In this manuscript, the MFMMS, magnetic and resistive measurements of Fe_3O_4 thin films are compared. An explanation of the physical origins of the features observed in the MFMMS is presented. This serves both as a study on the Verwey transition itself and as a technique for analyzing the MFMMS response of magnetic transitions in general.

The MFMMS signal is proportional to the surface resistance of a measured sample,

$$MFMMS \propto \frac{dR_S}{dH}, \tag{3.1}$$

which for metallic samples can be defined by

$$R_S = \frac{1}{\sigma\delta} = \sqrt{\frac{\mu\omega}{2\sigma}}, \tag{3.2}$$

where δ is the skin depth, μ is the real magnetic permeability of the material, ω is the microwave frequency and σ is the real component of the conductivity (*4*, *11*, *12*). When measured with an AC field, metallic samples are those with sufficiently low τ, the relaxation time of the material, for which $\omega\tau << 1$. For non-metallic samples, the imaginary component of the permeability and conductivity have non-negligible contributions, which will be addressed later. Because $\mu H = B = \mu_0(H+M)$, it is possible to derive a proportionality between the MFMMS signal and electromagnetic properties,

$$\frac{dR_S}{dH} = \sqrt{\frac{\rho\omega}{8\mu}} \times \left(\frac{d\mu}{dH} + \frac{\mu}{\rho}\frac{d\rho}{dH}\right). \tag{3.3}$$

To reduce this to more easily measurable properties, a geometric factor a can be defined such that $aR = \rho$ and $m/V=M$ holds, where V is the sample volume. Substituting these into equation 3.3,

$$\frac{dR_S}{dH} = \sqrt{\frac{a\omega\mu_0}{8V}} \times \left(\sqrt{\frac{R}{V+\frac{m}{H}}} \frac{H\frac{dm}{dH} - m}{H^2} + \sqrt{\frac{V+\frac{m}{H}}{R}} \frac{dR}{dH} \right) \tag{3.4}$$

can be derived. Notably, the right side of equation 3.4 is comprised only of known constants, R, dR/dH, M and dM/dH. These can be measured with isothermal magnetic hysteresis loops and magnetoresistance measurements from which the MFMMS signal can be calculated. For non-metallic samples, including Fe_3O_4 (*13*), there will be additional contributions to the absorbed microwave power from the imaginary components of the permeability and conductivity. This paper will ignore these contributions originating and determine what can be learned by comparing the MFMMS data to DC measurements. A discussion of the consequences of these assumptions will be presented at the conclusion of this manuscript.

3.3 Synthesis and Characterization

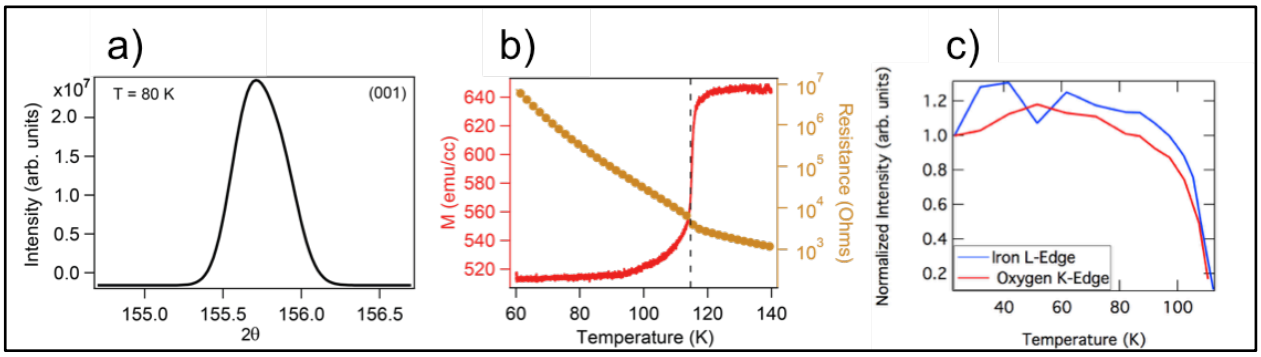

Figure 3.1: Characterization measurements for 50nm Fe_3O_4 thin films on MgO. (a) The structural integrity of the film characterized from the (001) Bragg peak from x-ray diffraction in the monoclinic phase. (b) Magnetic and resistivity measurements pinpoint the electronic Verwey transition temperature. (c) The integrated intensity of the (001/2) superlattice peak at the Fe L-edge and O K-edge resonant energies follows the monoclinic to cubic structural transition.

Thin film samples of Fe_3O_4 ranging from 50-100 nm in thickness were grown on MgO (001) substrates by reactive sputtering in an Ar/O_2 environment. The oxygen partial pressure during deposition was 0.1 mTorr while the total deposition pressure was 2 mTorr. MgO substrates were baked at 500 °C for 45 minutes prior to the deposition to ensure a good film-substrate interface. Subsequent x-ray diffraction measurements at 800eV of the Fe_3O_4 (001) peak (Fig. 3.1a) were used to characterize the structural quality.

The films showed the characteristic Verwey transition at 116 K as shown by the resistivity measurements in Fig. 3.1b (yellow curve). A change in magnetic moment was also observed near the phase transition in Fig. 3.1b (red curve) indicating the reorientation of the Fe magnetic moment. Both the resistivity and magnetization data are in agreement with literature (*14*, *15*)

The electronic Verwey transition is also accompanied by a structural transition from a high-temperature cubic phase to a low-temperature monoclinic phase. The monoclinic phase can be characterized by examining the (001) Bragg peak (Fig. 3.1a) that is forbidden in the cubic

phase. In addition, the signature of the (001/2) superlattice peak is only present in Bragg geometry in the monoclinic phase at the Fe L-edge and O K-edge resonant energies, and is a result of the lattice distortions in the monoclinic phase (*16–18*). The structural transition can be indirectly followed by monitoring the intensity of the superlattice peak at these resonant energies. The peak intensity disappears at about 115K (Fig. 3.1c), which is the approximate structural transition temperature.

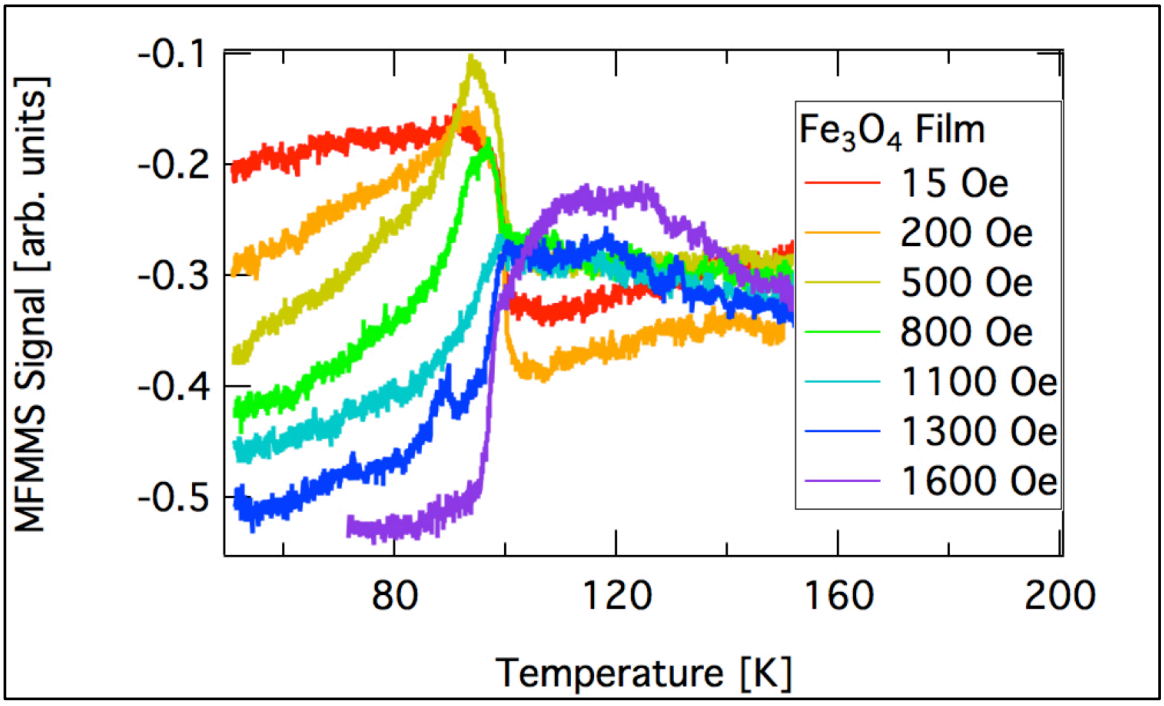

Figure 3.2: MFMMS temperature sweeps of Fe_3O_4 films at a range of DC fields and 15 Oe AC field, applied in parallel to the microwave magnetic field. Temperature was swept from low temperature to high during measurements.

These Fe_3O_4 thin films were mounted on quartz rods with vacuum grease and inserted into the MFMMS so that the magnetic fields are oriented in plane. They were then measured in the MFMMS with a range of applied DC magnetic fields, from 15 Oe to 1600 Oe and a fixed AC magnetic field of 15 Oe (Fig. 3.2). Measurements were taken on virgin samples with DC field strictly increasing between measurements. At 105 K, a step transition was observed in the MFMMS signal. At lower DC fields (800 Oe and below), the MFMMS signal sharply decreases

as temperature increases. At higher DC fields, the MFMMS signal sharply increases. Furthermore, at moderate fields (between 200 Oe and 800 Oe), there is a peak in the MFMMS signal below 105 K. This switching step transition and peak in the MFMMS signal is likely caused by the Verwey transition. From this data alone, it is impossible to determine the physical origins of the peak and the switching step transition. Because Fe_3O_4 is not metallic, equation (3.4) will describe only some components of the MFMMS behavior, though data calculated using that equation will still be useful for analyzing the MFMMS data. Furthermore, even without consulting equation (3.4), separate measurements of the resistive and magnetic properties can be compared to the MFMMS data to deduce the physical origin of these features. Note that 105 K is lower than one would expect for the Verwey transition. This is attributed mostly to microwave heating of the magnetite particles, as previously observed (*19*), although 1-2 K of the offset could be the result of a thermal offset between the sample and thermometer in the flow cryostat.

To investigate how the DC electric and magnetic behavior of the sample contributes to the MFMMS signal, a series of isothermal magnetic hysteresis loops and magnetoresistance measurements were taken. These measurements ranged from 90 K to 145 K with the highest measurement density between 110 K and 115 K, where the Verwey transition was observed in these measurements. To construct plots showing magnetic and resistive properties as a function of temperature, data points were taken from each isothermal measurement, at a given magnetic field (see supplementary information). In this way, resistive and magnetic properties, as well as the magnetic field derivatives of those properties could be plotted against temperature at a range of magnetic fields (Fig. 3.3).

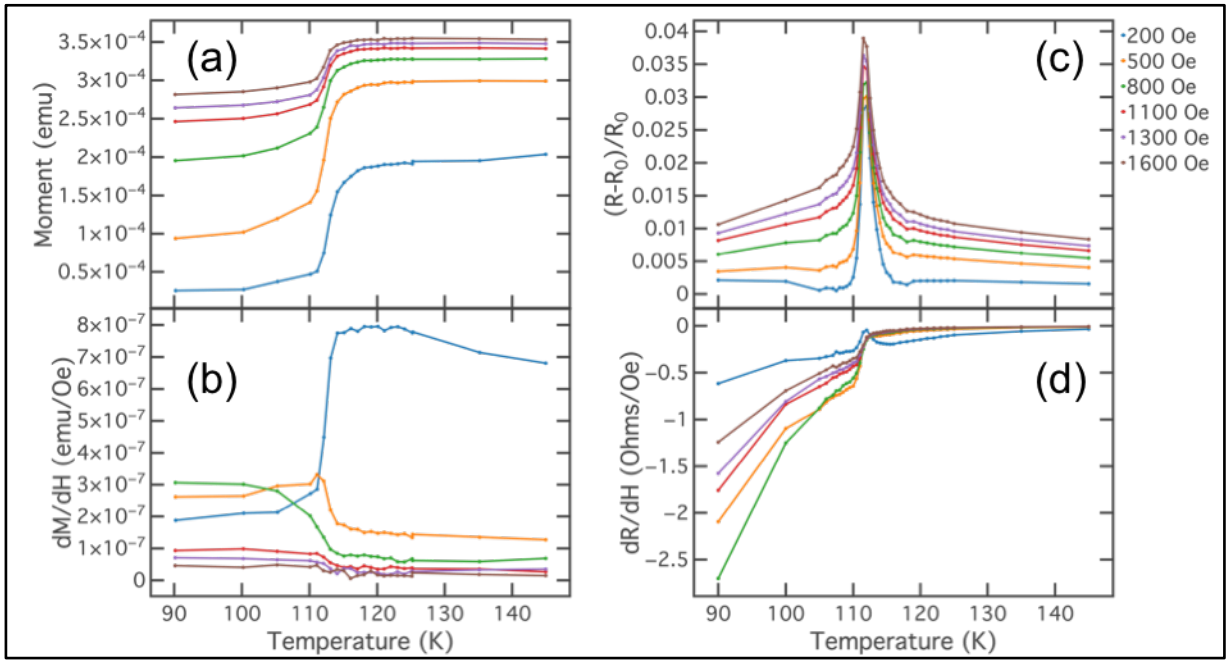

Figure 3.3: Magnetic and resistive behavior of Fe_3O_4 thin films as a function of temperature. Magnetic moment (a), its derivative with magnetic field (b), magnetoresistance (c) and the magnetic field derivative of the resistance (d) are presented at a range of applied DC fields (200 Oe – 1600 Oe). Data is taken from isothermal magnetic hysteresis loops and magnetoresistance measurements (Fig. 3.5).

The magnetic moment in these films sharply increases with increasing temperature at the Verwey transition (Fig. 3.3a). This is true at all fields, although it is amplified at higher fields. The magnetic field derivative of the magnetic moment sharply increases with increasing temperature at low fields (Fig. 3.3b). However, at higher fields, the magnetic field derivative of the magnetic moment decreases with increasing temperature. This is similar to the switching step behavior observed in the MFMMS, which indicates that the switching step behavior is a result of the magnetic properties of the thin film.

There is a sharp peak in the magnetoresistance at all fields at the Verwey transition (Fig. 3.3c) which is a known feature of magnetite (*20*). The magnetic field derivative of the resistance also has a peak at lower applied magnetic fields (Fig. 3.3d). It is unclear which of these is responsible for the peak in the MFMMS behavior, but the peak is clearly related to the resistive

properties of the film. Combined, these figures demonstrate the behavior observed in the MFMMS: there is a switching step behavior in the magnetic properties of the film, and a peak in the resistive properties.

3.4 Discussion

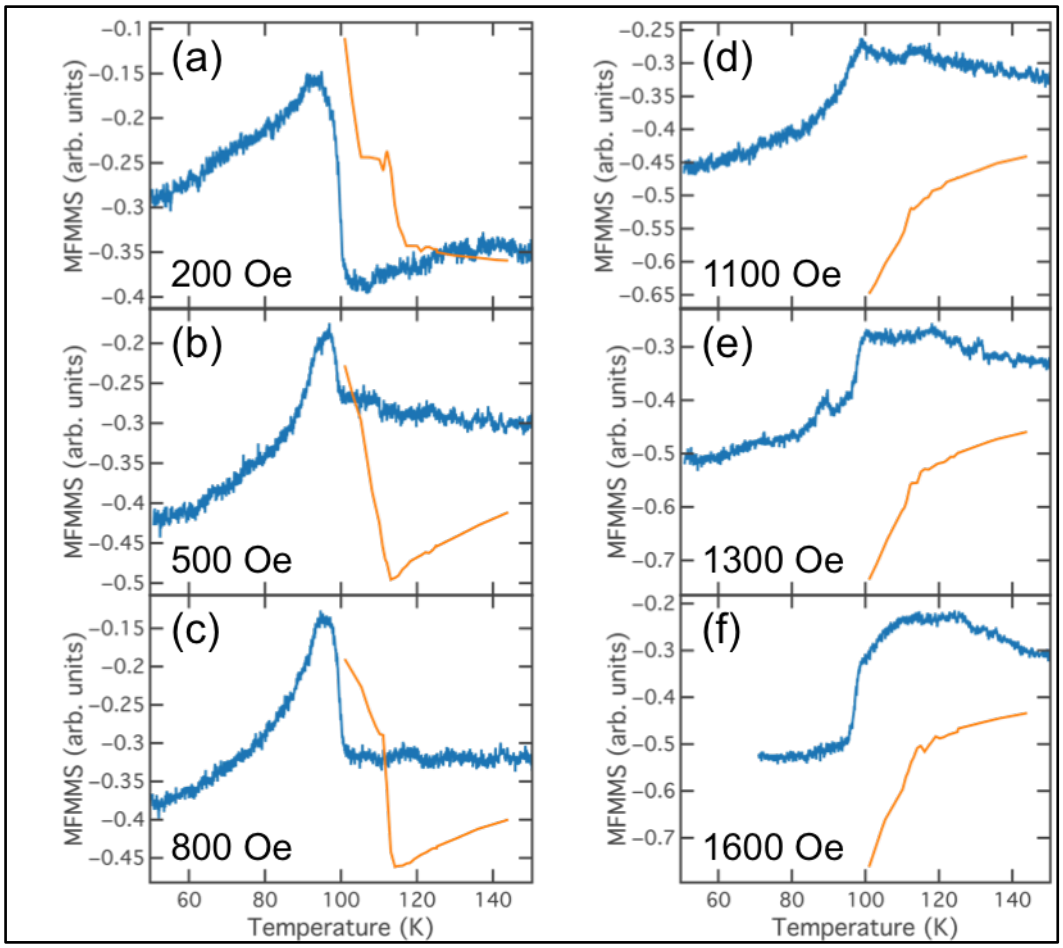

Figure 3.4: MFMMS measurements of Fe_3O_4 thin films (blue) and data calculated from magnetic and resistive data (orange). Measurements are presented with a range of DC magnetic fields (a-f). To facilitate this comparison, calculated data is vertically scaled and offset. Note that the difference in the transition temperatures observed in experimental and calculated data is a result of the MFMMS flow cryostat (see above).

Using this data and equation (3.4), it was possible to calculate an expected MFMMS signal. To do this, the data in Fig. 3.3 was linearly interpolated, to allow for easy calculation, and then inserted into equation (3.4). This was done for the complete temperature range for each field

in Fig. 3.3. To compare this calculated MFMMS data to the experimental MFMMS data, the calculated data was rescaled and shifted vertically (Fig. 3.4). It should be noted that the calculated MFMMS data is not expected to exactly model the experimental data. This is true first Fe_3O_4 is not a metal and equation (3.4) does not model complex contributions to permeability and conductivity. Furthermore, as equation (3.2) shows, the surface resistance depends on the skin depth of a material. When measuring a thin film, the skin depth can be comparable or larger than the film thickness, which decreases the accuracy of the model. However, by comparing the calculated data to the experimental data, similarities can still be analyzed.

The calculated data is particularly successful at reproducing the high temperature behavior of the experimental data. The transitions in the calculated and experimental MFMMS data have the same sign at each field. The step transition switches its sign between 800 Oe and 1100 Oe in both the calculated and experimental data. Furthermore, the shape of the high temperature behavior with relation to the transition is similar. However, there are some significant differences, most noticeably in the low temperature behavior. In addition, while there is a peak observed in the calculated data at 200 Oe, it is much smaller than that observed in the experimental data and does not persist to higher fields. Despite these differences, it is clear that the peak behavior observed in the MFMMS is a result of the resistive properties of the film and the switching step function is a result of the magnetic properties of the film.

The failure to perfectly reproduce the data is likely due to the limitations of the assumptions of the technique – that is, it assumes a metallic non-superconducting sample with a microwave permeability equal to its DC permeability. These assumptions will rarely be completely true in non-metallic samples, but as this Fe_3O_4 study demonstrates, it is still possible to draw useful conclusions even when the assumptions are partly untrue. While the calculated

MFMMS data does not perfectly reproduce the experimental data, it explains which of the features observed in the MFMMS can be explained by the DC magnetic and resistive behavior. This is important because when measuring non-superconducting materials, understanding the MFMMS signal has previously been an intractable problem. This technique will allow the measurement and analysis of other non-superconducting transitions in the MFMMS and while it will only be able to thoroughly analyze good metals, it still provides a quick way to gain insight about other samples. This is crucial, because MFMMS is best used as a first screening technique, quickly taking highly sensitive measurements of both majority and minority phases of samples. While it fulfills that role for superconducting samples, it has been difficult until now to properly study other electromagnetic phase transitions in this system. Given that the technique is already more sensitive than competing techniques, increasing the analysis capabilities of the MFMMS will open new avenues of research.

3.5 Supplementary Information - Methods

3.5.1 Magnetic hysteresis loops and Magnetoresistance

Thin films were measured in a PPMS with the film oriented so that the magnetic field was in plane. Magnetoresistance measurements were performed with the current parallel to the field. While full hysteresis loops were measured, only the virgin curves were compared to the MFMMS, because these measurements mimicked the measurement conditions of the MFMMS (ie: all of these measurements involved virgin samples being measured under strictly increasing magnetic field).

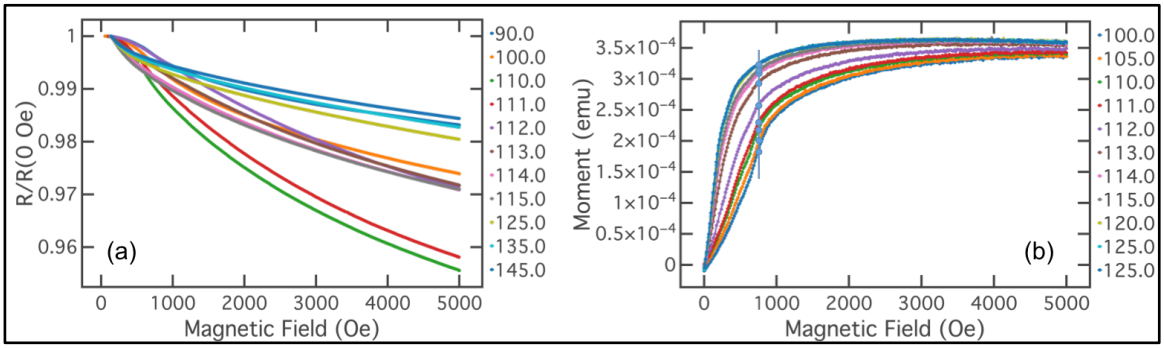

Figure 3.5: Virgin branches of isothermal magnetoresistance loops (a) taken with parallel geometry. Virgin branches of magnetic hysteresis loops (b) with a vertical line highlighting points taken at 1000 Oe (see below). For both (a) and (b), only a selection of the data taken is included in the figure, for visual clarity.

In order to obtain magnetic and resistive properties as a function of temperature (Fig. 3.3), one point was taken from each measurement at the appropriate magnetic field, as shown in Fig. 3.5b. If a point did not exist at exactly the desired field, it was interpolated from the nearest points. These points were then combined to form a composite curve, which showed a resistive or magnetic property plotted against temperature (for example, the points highlighted in Fig. 3.5b combine to show magnetic moment vs. temperature at 800 Oe)

In order to reduce the noise in the derivatives, *dR/dH* and *dM/dH* were calculated by first smoothing the raw data with a Savitzky–Golay filter (*21*) and then calculating the numerical derivative using a 7^{th} order central difference formula. The filter had a width of 19 points, was 3^{rd} order, and was performed twice on resistance data and 20 times on magnetic moment data. Smoothed data was checked thoroughly to ensure that no data loss happened due to smoothing.

3.5.2 Calculated MFMMS data

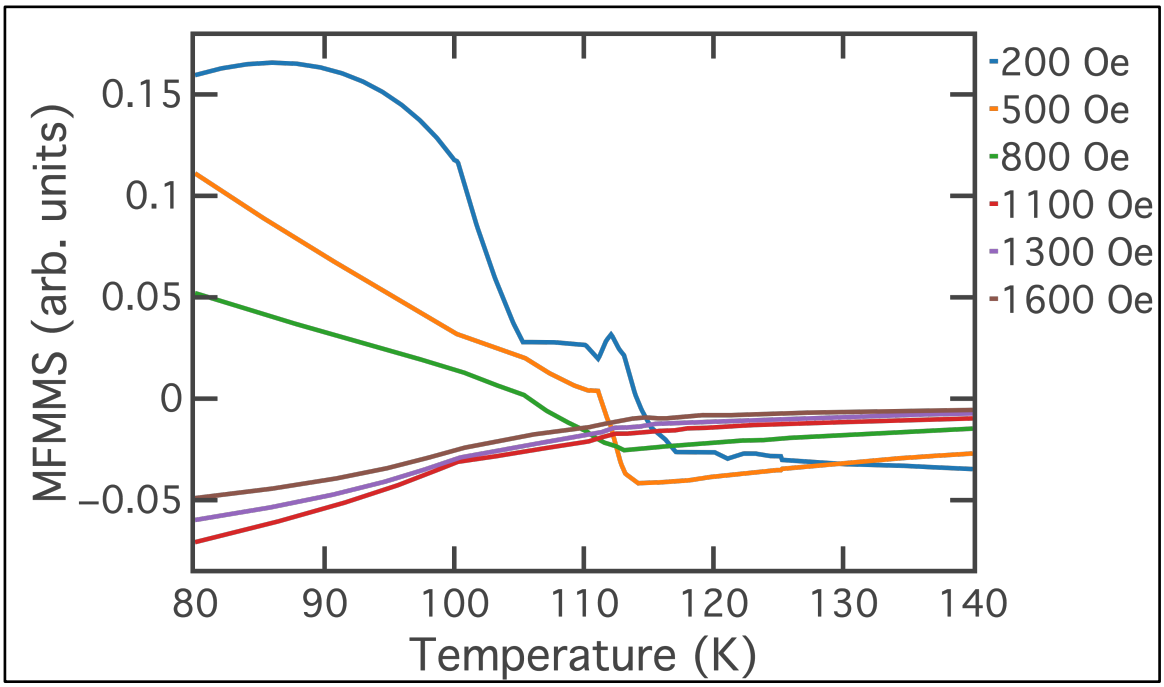

Figure 3.6: Calculated MFMMS data, created using equation (3.4) with fixed DC field (see legend). The data presented in this figure was taken to create the calculated data in Fig. 3.4.

In order to create the calculated MFMMS data, the curves shown in Fig. 3.3 were more densely populated, by linearly interpolating the existing data at regular temperature intervals. This data was then inserted into equation (3.4). The result of this process was Fig. 3.6.

3.6 Acknowledgements

Chapter 3 was prepared based on material that is to be submitted for publication: Wampler, James; Hua, Nelson; Kukreja, Roopali; Ramirez, Juan Gabriel; Basaran, Ali; Fullerton, Eric; Shpyrko, Oleg; Schuller, Ivan K. “The Electromagnetic Origin of the Microwave Absorption Response of Fe3O4 Thin Films.” J. W. was the principal researcher/author on this paper.

3.7 References

1. K. W. Blazey, K. A. Müller, J. G. Bednorz, W. Berlinger, Low-field microwave absorption in the superconducting copper oxides. *Phys. Rev. B*. **36**, 7241 (1987).

2. K. W. Blazey, A. M. Portis, A. Dulcic, B. Rakvin, M. Pozek, I. Ciccarello, M. Guccione, F. I. Limits, S. Calatroni, R. Vaglio, Microwave Magneto-Surface Impedance of High- Tc Superconductors. *Europhys. Lett.* **5**, 467 (1988).

3. G. K. Padam, S. N. Ekbote, M. R. Tripathy, Srivastava G P, B. K. Das, Non-resonant microwave absorption studies in $Bi_{1.6}Pb_{0.4}Sr_2Ca_2Cu_3O_{10+x}$. *Phys. C*. **315**, 45 (1999).

4. J. G. Ramírez, A. C. Basaran, J. de la Venta, J. Pereiro, I. K. Schuller, Magnetic field modulated microwave spectroscopy across phase transitions and the search for new superconductors. *Reports Prog. Phys.* **77**, 093902 (2014).

5. R. K. Kremer, B. Kanellakopulos, P. Bele, H. Brunner, F. A. Neugebauer, Weak ferromagnetism and magnetically modulated microwave absorption at low magnetic fields in 1,3,5-triphenyl-6-oxoverdazyl. *Chem. Phys. Lett.* **230**, 255 (1991).

6. G. Alvarez, R. Font, J. Portelles, R. Zamorano, R. Valenzuela, Microwave power absorption as a function of temperature and magnetic field in the ferroelectromagnet Pb (Fe1 / 2 Nb1 / 2) O3. *J. Phys. Chem. Solids*. **68**, 1436 (2007).

7. T. Saerbeck, J. Pereiro, J. Wampler, J. Stanley, J. Wingert, O. G. Shpyrko, I. K. Schuller, Ferromagnetism in partially oxidized CuCl. *J. Magn. Magn. Mater.* **346**, 161 (2013).

8. M. P. Gutiérrez, G. Alvarez, H. Montiel, R. Zamorano, R. Valenzuela, Study of the Verwey transition in magnetite by low field and magnetically modulated non-resonant microwave absorption. *J. Magn. Magn. Mater.* **316**, e738 (2007).

9. F. Walz, The Verwey transition - a topical review. *J. Phys. Condens. Matter*. **14**, R285 (2002).

10. S. Guénon, J. G. Ramírez, A. C. Basaran, J. Wampler, M. Thiemens, S. Taylor, I. K. Schuller, Search for superconductivity in micrometeorites. *Sci. Rep.* **4**, 7333 (2014).

11. F. J. Owens, C. P. J. Poole, in *Electromagnetic Absorption in the Copper Oxide Superconductors* (Kluwer Academic Publishers, New York, Boston, Dordrecht, London, Moscow, 1999), pp. 75–84.

12. C. V. Topping, S. J. Blundell, A.C. susceptibility as a probe of low-frequency magnetic dynamics. *J. Phys. Condens. Matter*. **31** (2019), doi:10.1088/1361-648X/aaed96.

13. S. Ni, X. Sun, X. Wang, G. Zhou, F. Yang, J. Wang, D. He, Low temperature synthesis of Fe_3O_4 micro-spheres and its microwave absorption properties. *Mater. Chem. Phys.* **124**, 353 (2010).

14. D. T. Margulies, F. T. Parker, F. E. Spada, R. S. Goldman, J. Li, R. Sinclair, A. E. Berkowitz, Anomalous moment and anisotropy behavior in Fe_3O_4 films. *Phys. Rev. B*. **53**, 9175 (1996).

15. G. Q. Gong, A. Gupta, G. Xiao, W. Qian, V. P. Dravid, Magnetoresistance and magnetic

properties of epitaxial magnetite thin films. *Phys. Rev. B*. **56**, 5096 (1997).

16. S. B. Wilkins, S. Di Matteo, T. A. W. Beale, Y. Joly, C. Mazzoli, P. D. Hatton, P. Bencok, F. Yakhou, V. A. M. Brabers, Critical reexamination of resonant soft x-ray Bragg forbidden reflections in magnetite. *Phys. Rev. B*. **79**, 2 (2009).

17. J. Schlappa, C. Schüßler-Langeheine, C. F. Chang, H. Ott, A. Tanaka, Z. Hu, M. W. Haverkort, E. Schierle, E. Weschke, G. Kaindl, L. H. Tjeng, Direct observation of t_{2g} orbital ordering in magnetite. *Phys. Rev. Lett.* **100**, 1 (2008).

18. R. Kukreja, N. Hua, J. Ruby, A. Barbour, W. Hu, C. Mazzoli, S. Wilkins, E. E. Fullerton, O. G. Shpyrko, Orbital Domain Dynamics in Magnetite below the Verwey Transition. *Phys. Rev. Lett.* **121**, 177601 (2018).

19. F. Sakran, A. Copty, M. Golosovsky, D. Davidov, P. Monod, Scanning ferromagnetic resonance microscopy and resonant heating of magnetite nanoparticles: Demonstration of thermally detected magnetic resonance. *Appl. Phys. Lett.* **84**, 4499 (2004).

20. X. W. Li, A. Gupta, G. Xiao, G. Q. Gong, Transport and magnetic properties of epitaxial and polycrystalline magnetite thin films. *J. Appl. Phys.* **83**, 7049 (1998).

21. A. Savitzky, M. J. E. Golay, Smoothing and Differentiation of Data by Simplified Least Squares Procedures. *Anal. Chem.* **36**, 1627 (1964).

Chapter 4 – Searching for superconductivity in doped Sr_2IrO_4 using MFMMS

4.1 Bulk powder samples for measurement in MFMMS

Because MFMMS can quickly screen samples for the presence or absence of superconductivity, sample synthesis is frequently the bottleneck to research. Chapter 2 discussed one solution to this problem: measuring natural samples removes the need to synthesize samples. This can allow for rapid measurement of a wide range of material phases. However, many phases do not form naturally, and in order to measure these phases, it is necessary to synthesize them. One of the most efficient ways to do this is through powder metallurgy.

Powder metallurgy synthesis is a broad term describing a range of techniques, but is generally a process that involves mixing together powders in different ratios and heating in specific gaseous environments. The work described here involves manually mixing powders and heating them in tube furnaces. Using this technique, maximum temperature, heating rate, bake time, cooling rate and gaseous ratios can all be tuned to successfully produce samples. In these sorts of techniques, it is sometimes necessary to grind up initial products and reheat them, in order to achieve phase pure samples (*1*, *2*). These last steps are not usually necessary for MFMMS measurements however, since it is capable of detecting superconducting transitions within minute phases of inhomogeneous samples, as discussed in chapter 1. This chapter discusses the study of doped Sr_2IrO_4 samples synthesized using the techniques described above and the investigation of a superconducting minority phase in the powder samples.

4.2 Motivation

While there are no predictive rules in the search for high-T_c superconductivity, good empirical guidelines can potentially help increase the odds of successfully finding new compounds. Many recent superconducting discoveries have been found in layered compounds

with light elements (*3*, *4*). In addition, there has been success in finding superconductivity in doped, multi-element compounds (*5*–*7*), although there are notable examples of binary high-T_c superconducting compounds, such as MgB_2 and H_2S (*8*, *9*).

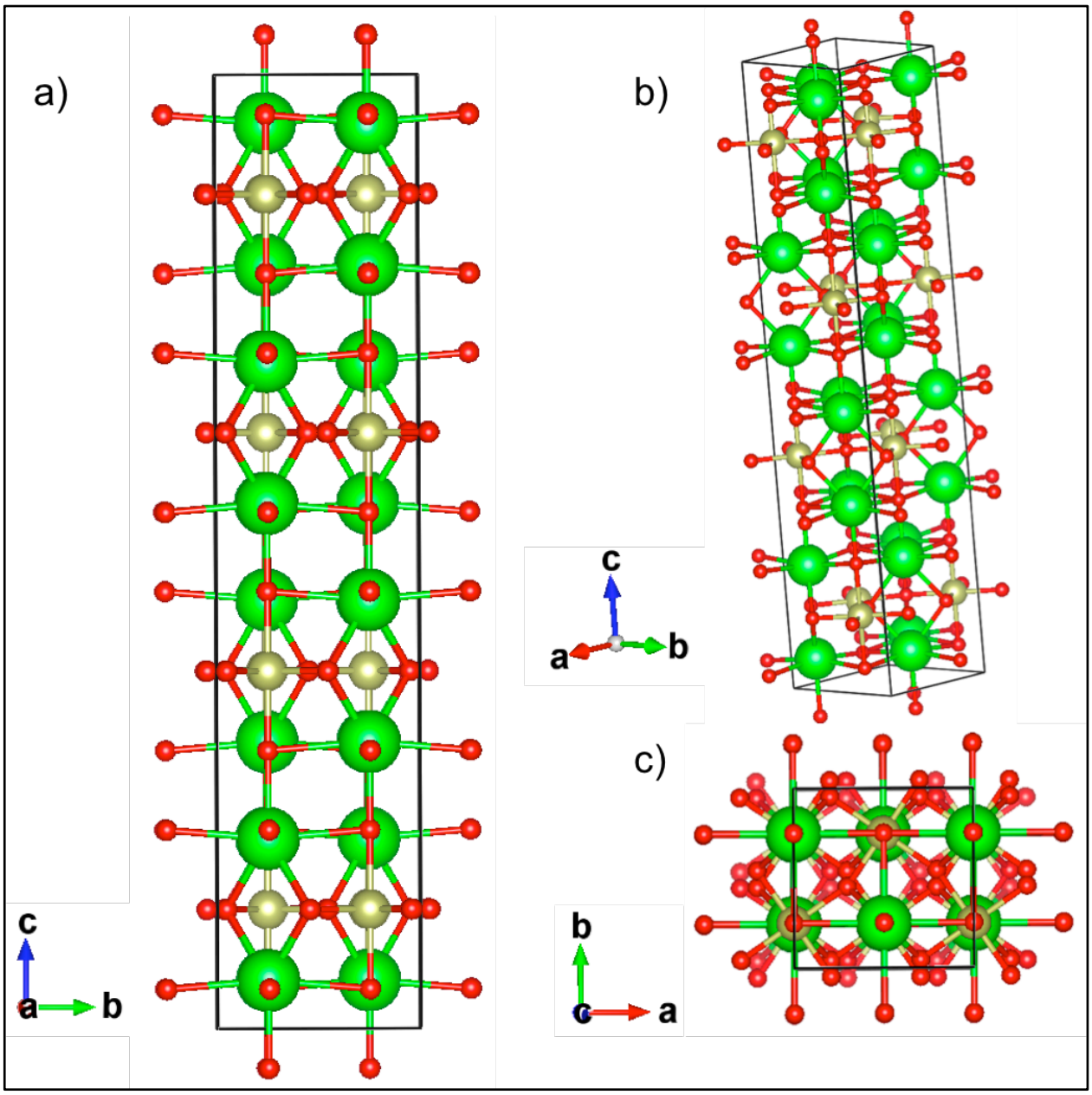

Figure 4.1: Sr_2IrO_4 crystal structure pictured from three different angles. Green atoms are Sr, beige are Ir, red are O. Drawings made with VESTA (*15*).

Following these rules, doped Sr_2IrO_4 (strontium iridate) is a promising candidate family of phases to search for superconductivity. Sr_2IrO_4 has a Perovskite structure with Ir-O and Sr-O layers (Fig. 4.1). Sr_2IrO_4 is a paramagnet at high temperatures, but exhibits weak ferromagnetism below ~225 K. This weak ferromagnetism is a product of the spin lattice's canted antiferromagnetism (*10*). In addition to being a layered multi-element compound with light elements, it is crystollographically and electronically similar to the cuprates (*10*, *11*). There have been many suggestions that either electron- (*12*, *13*) or hole- (*14*) doped Sr_2IrO_4 may contain superconductivity. Particularly notable is the *d*-wave gap observed in electron-doped Sr_2IrO_4 (*13*).

4.3 Sample Synthesis

Undoped Sr_2IrO_4 samples were grown from a powder mixture of $SrCO_3$ and IrO_2 with a 2:1 ratio. These powders were ground with a mortar and pestle and then stirred so that they were thoroughly mixed. This powder mix was heated in a quartz boat and alumina tube in a tube furnace. It was heated at a rate of 100 °C/h until it reached a maximum temperature of 1000 °C. It was sintered at this temperature for 24 h and then the power was shut off and the sample was allowed to cool thermally. This was done with a low gas flow of 20 sccm Ar and 5 sccm O_2. In order to further minimize gas flow through the sample area, the gas input and output were on the same side of the tube furnace. This flow of gas was low enough that reactants with a high vapor pressure were not blown away from the middle of the tube furnace. Previous work has shown that a 2:1 ratio of Sr and Ir with near atmospheric conditions can produce Sr_2IrO_4 at these temperatures (*16*) and doped and undoped polycrystalline Sr_2IrO_4 powder samples have been formed with these reactants at these temperatures (*14*). After baking, the power was shut off and the sample was allowed to cool slowly. This procedure resulted in samples with the desired

phase (as shown in the x-ray data below), but not the phase pure samples that might be obtained by multiple grinding and baking steps. These impure samples are ideal for MFMMS measurement, since it is capable of measuring very small impurity phases for superconducting transitions.

In order to create doped samples, chemicals containing additional elements were mixed into the $SrCO_3$ – IrO_2 mixture. A quantity of $SrCO_3$ or IrO_2 was replaced by an amount of dopant with an equal molar concentration, depending on whether the element was intended to be doped into the Sr- or Ir-site in the Sr_2IrO_4 lattice (Table 4.1). The additional chemicals mixed in were metals or metal oxides in varying oxidation states. Because of the excess of oxygen in the atmosphere above the samples, the product fully oxidized in the oven regardless of the oxidation state of the dopant chemical. As a result, dopant chemicals were chosen based on chemical stability and ease of use.

Table 4.1: Chemically doped Sr_2IrO_4 samples made via powder metallurgy. "Samples" indicates the percentage of dopant used in each sample made with that particular dopant. Each percentage listed is a distinct sample.

Dopant	Chemical Used	Dopant Site	Samples (%)
Pt	PtO_2	Ir	5, 10, 20
Os	OsO_2	Ir	10, 20
Rh	Rh	Ir	10
Rb	Rb_2CO_3	Sr	10
La	La_2O_3	Sr	10, 20

4.4 X-ray

In order to determine the crystal structure of the majority phase of the samples, X-ray diffraction (XRD) measurements were taken of each of the doped and undoped samples. Powder samples on slides were characterized with a Rigaku SmartLab 1-D X-ray Diffractometer. A

parallel beam geometry was used, measuring from 3° to 120° in 2θ. A monochrometer was not used, so as to ensure a sufficiently high number of counts were measured by the detector.

These measurements were compared to idealized Sr_2IrO_4 XRD data taken from the Inorganic Crystal Structure Database (ICSD) (*17*). The undoped sample had peaks that matched every peak observed in the idealized data (Fig. 4.2). It also had additional peaks, which are attributed to minority phases. Because MFMMS is much more sensitive than these crystallography measurements, if any of the minority phases that could be observed in the XRD data are superconducting, this transition would likely be measurable using MFMMS.

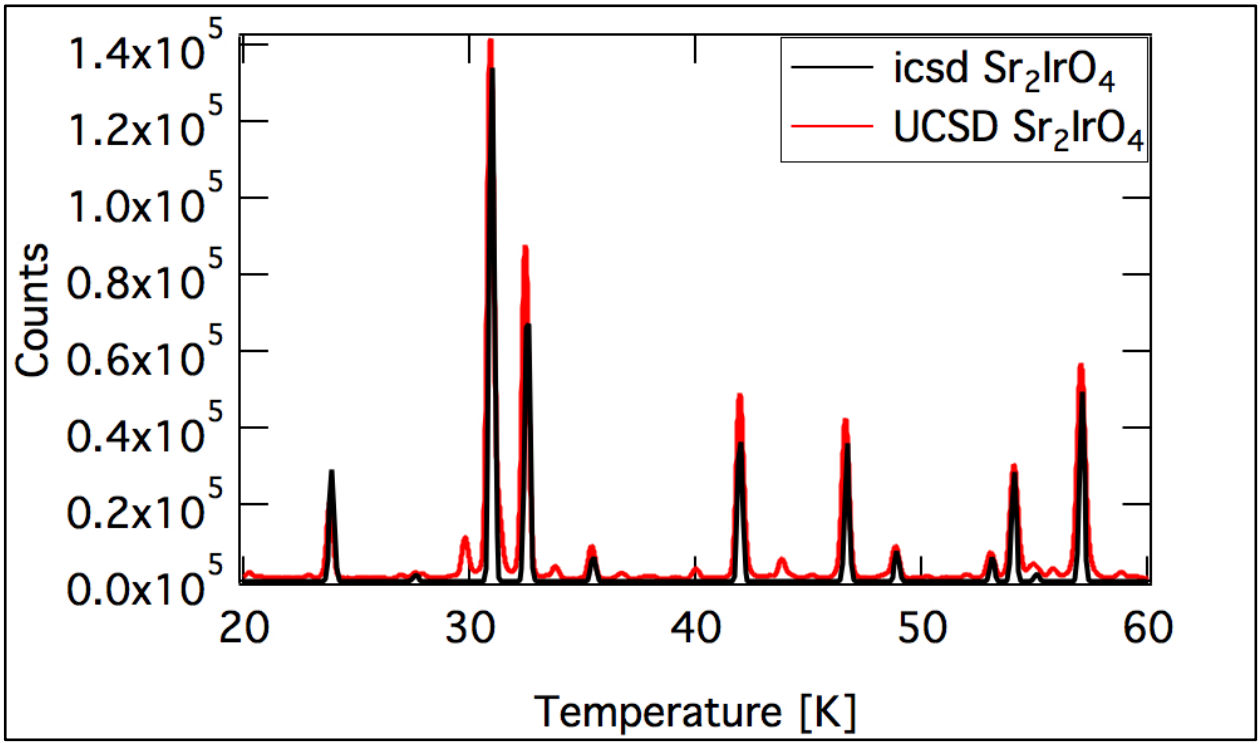

Figure 4.2: XRD measurements of undoped Sr_2IrO_4 powder sample, compared to idealized data from ICSD. ICSD data is vertically scaled for the purposes of comparison.

Similar measurements were taken on each of the doped samples (Fig. 4.3). Sr_2IrO_4 peaks were observed in each of them. This fact means that a structure was synthesized in the doped sample with the crystallinity of Sr_2IrO_4, but not that the added chemical was successfully doped

into this structure. Just above and below $2\theta = 20°$, two minor peaks can be observed in some of the doped samples, most significantly in the $Sr_2Ir_{0.8}Os_{0.2}O_4$ and $Sr_{1.6}La_{0.4}IrO_4$ samples. These minor peaks do not appear in the undoped sample nor do they appear in the idealized Sr_2IrO_4 peaks (Fig. 4.2). This means that these two doped samples have a significant minority phase. The rest of the doped samples (which do not have any significant minor peaks that do not appear in the undoped sample) do not have such a minority phase. The lack of substantial minority phases implies that the chemical doping was successful for all except the $Sr_2Ir_{0.8}Os_{0.2}O_4$ and $Sr_{1.6}La_{0.4}IrO_4$ samples. For these two samples, this data is insufficient to determine if the doping was successful. In order to confirm this and investigate these samples further, we took MFMMS and magnetic measurements.

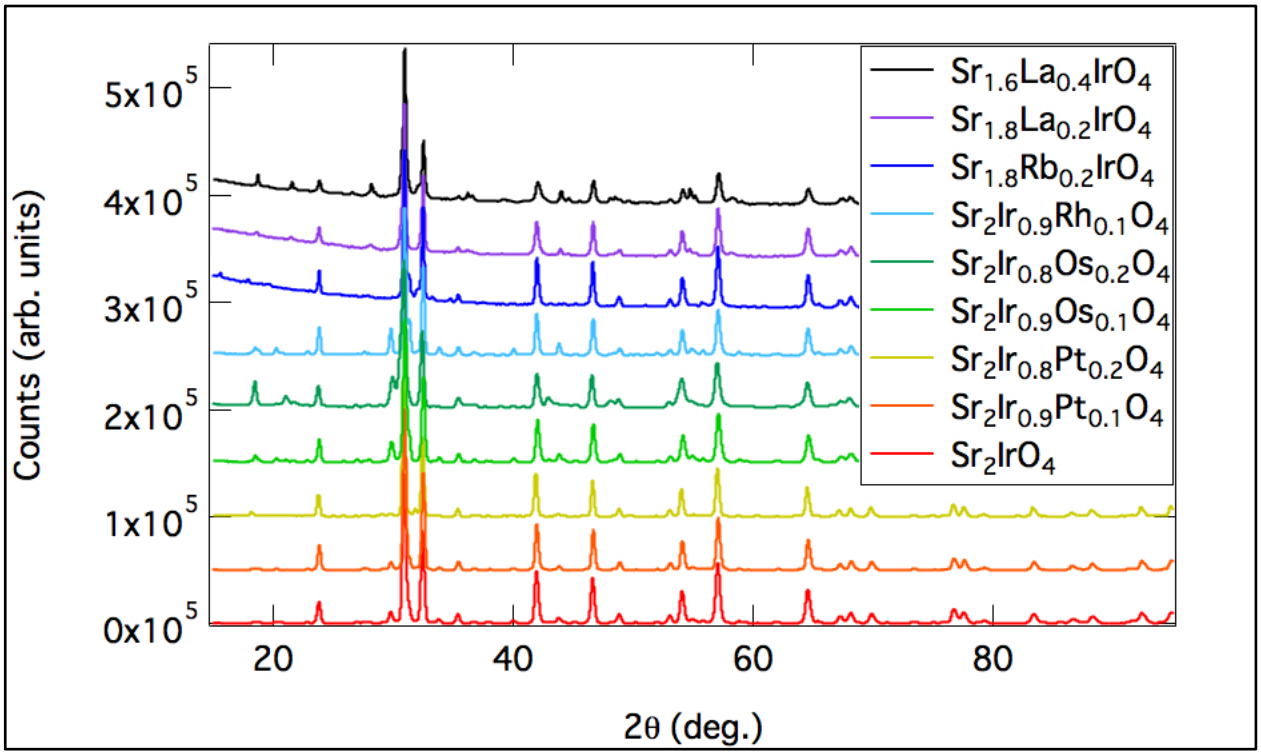

Figure 4.3: XRD measurements of undoped and doped Sr_2IrO_4 powder sample. Data is vertically scaled and offset for the purposes of comparison.

4.5 MFMMS Measurements

Approximately 1 mm^3 of powder was inserted into 4 mm radius quartz tubes in order to prepare samples for MFMMS measurements. MFMMS measurements were taken with an AC field of 15 Oe, and a DC offset field ranging from 15 Oe to 2000 Oe. Initial measurements were generally taken of the whole temperature range, between ~280 K and ~4 K, with a DC offset field of 15 Oe, at a scan speed of approximately 5 K/min. Subsequent measurements either increased the DC field to observe the sample behavior at higher fields, or restricted the temperature range to focus on an apparent feature in the MFMMS signal.

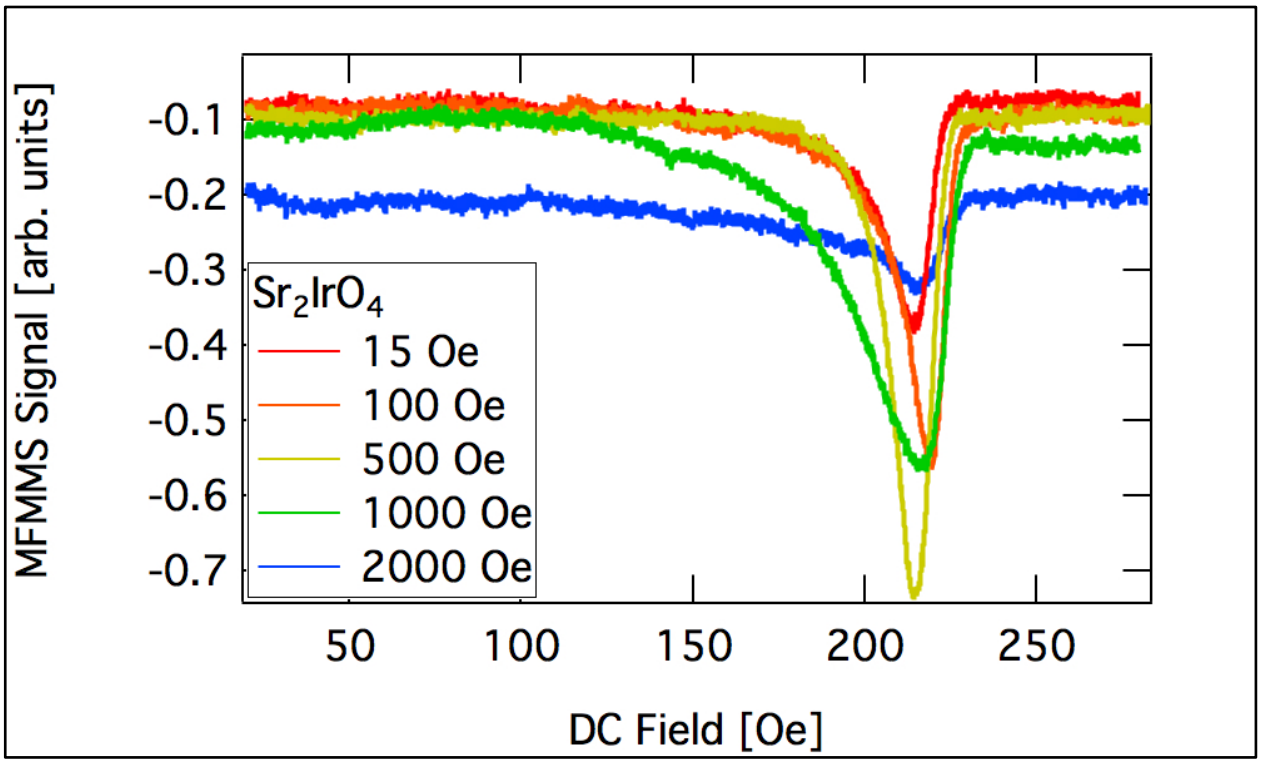

Figure 4.4: MFMMS measurements of an undoped Sr_2IrO_4 sample, with a range of applied DC fields. DC field ranges from 15 Oe to 2000 Oe. Measurements were taken with a scan speed of ~5 K/min.

In the undoped sample, there is a dip in the MFMMS data at about 225 K (Fig. 4.4). This dip is amplified by applying a moderate DC field, up to H_{DC} = 500 Oe. At 1000 Oe and above, the dip is suppressed in magnitude. The onset temperature of this dip is not significantly affected

by changing the applied DC field. This dip is attributed to the magnetic transition from paramagnetism to weak ferromagnetism reported in the literature, since its onset temperature is the same as the magnetic transition temperature. (*10*)

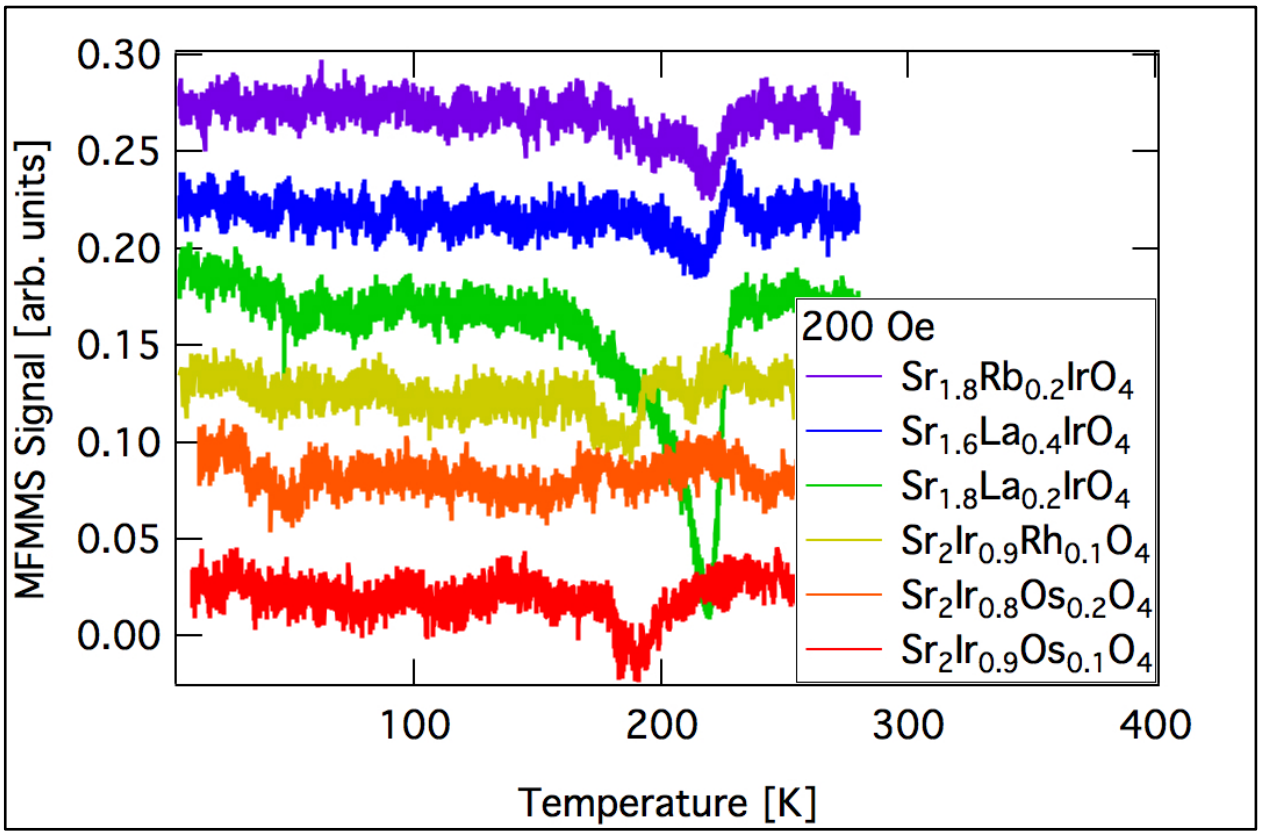

Figure 4.5: MFMMS measurements of Rb-, La-, Rh- and Os-doped Sr_2IrO_4 samples with an applied DC field of 200 Oe. Measurements were taken with a scan speed of ~5 K/min. Data is vertically offset for visual clarity.

In most of the doped samples (Fig. 4.5), there were no new features that were observed in the MFMMS measurements. The magnetic transition was observed in the MFMMS measurements of some of the Rb-, La-, Rh- and Os- doped samples, though it was not observed in all of them. Even in those samples that exhibited the magnetic transition, in all the samples except for the $Sr_{1.6}La_{0.4}IrO_4$, the magnetic transition was nearly completely suppressed. Since it is not clear from the X-ray data that the doping was successful in that sample, it is not possible to

conclude anything from this exception. In general though, the magnetic transition appears to be suppressed in the doped samples.

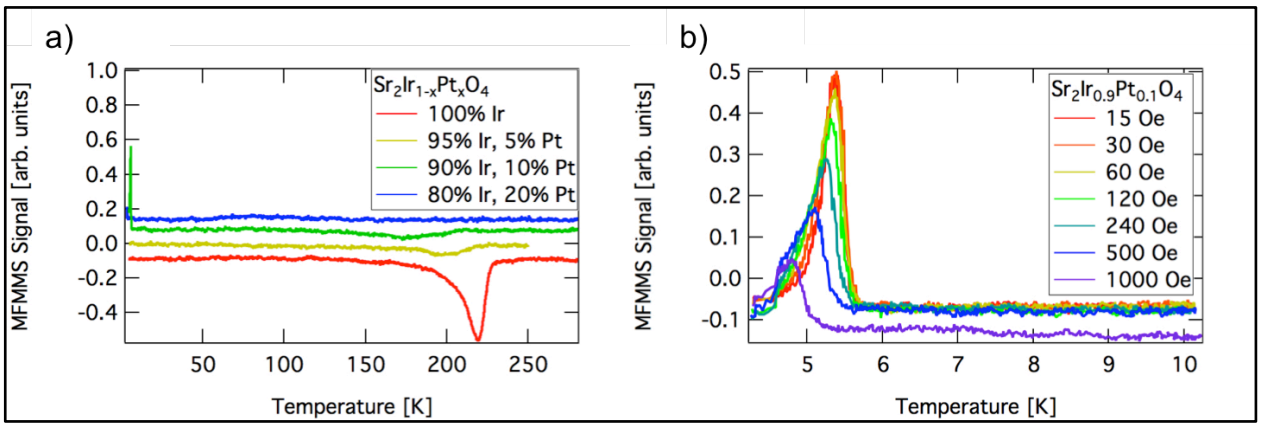

Figure 4.6: MFMMS measurements of Pt-doped Sr_2IrO_4 samples. Samples with Pt-concentrations ranging from 0% to 20% were measured from 280 K to 4 K at a scan speed of ~5 K/min with an applied DC field of 100 Oe (a). These measurements are vertically offset for clarity. Low temperature measurements on a sample with a Pt-concentration of 10% were measured from 10K to 4K at a scan speed of ~1 K/min (b). Applied DC fields ranged from 15 Oe to 1000 Oe.

While the MFMMS measurements of the Pt-doped samples exhibit a similar suppression of the magnetic transition, there is also a peak in the MFMMS measurements of the $Sr_2Ir_{0.9}Pt_{0.1}O_4$ and $Sr_2Ir_{0.9}Pt_{0.2}O_4$ samples at low temperature (Fig. 4.6a). In order to probe this feature, a series of measurements was taken with the DC offset field varying from 15 Oe to 1000 Oe (Fig. 4.6b). In order to reduce the thermal offset caused by the flow cryostat in MFMMS, temperature was swept slowly, at a speed of only 1 K/min. At this slow scan speed, the onset temperature of the peak was 5.7 K. As the DC field was increased, the peak in the MFMMS signal was suppressed, both in magnitude and in onset temperature. This MFMMS behavior is characteristic of a superconducting transition, as previously exhibited by Nb thin films (*18*). Note that because this signal is very small, it is almost certainly not produced by the majority phase in the sample. Three MFMMS samples were measured from the $Sr_2Ir_{0.9}Pt_{0.1}O_4$ parent sample and of

these, two exhibited this peak transition. This suggests that the superconducting phase is irregularly distributed throughout the parent sample.

4.6 Magnetic Measurements

The sample measured in Fig. 4.6 were removed from the quartz tubes used in MFMMS by breaking the tubes just above the bottom and scraping out the powder. This powder was then measured using vibrating sample magnetometry (VSM) in order to determine if the superconducting minority phase observed via MFMMS could be measured with this technique – and to characterize it if this was possible. An undoped sample was also measured for comparison.

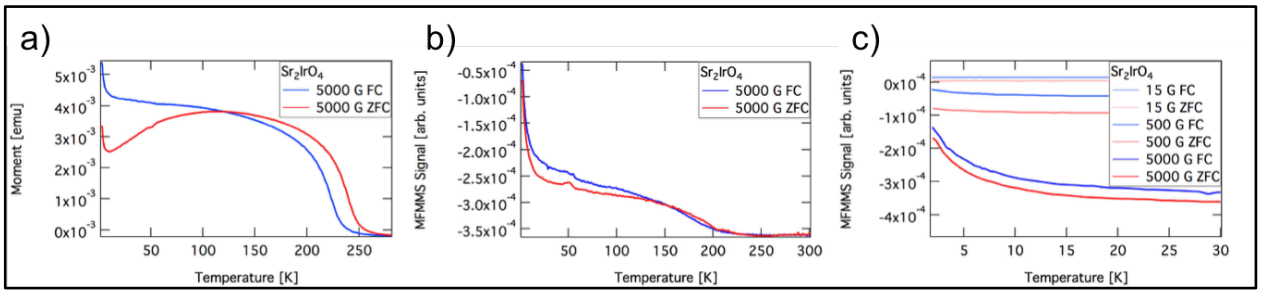

Figure 4.7: VSM measurements of undoped (a) and Pt-doped (b,c) Sr_2IrO_4 samples. Zero field cooled (ZFC) measurements (blue curves) were performed first with increasing temperature. Field cooled (FC) measurements were performed second with decreasing temperature. Applied magnetic field was 5000 G (a, b) or ranged from 15 G to 5000 G (c), depending on the measurement. In the latter case (c), measurements were vertically offset for clarity.

In both undoped (Fig. 4.7a) and doped (Fig. 4.7b) samples, the weak ferromagnetic transition can be observed above 200 K with 5000 G applied field. It is somewhat suppressed in temperature in the Pt-doped sample, as observed in MFMMS measurements of doped Sr_2IrO_4 samples. Thermal hysteresis can be observed in the onset of the weak ferromagnetism. In addition, a sharp increase can be observed in the moment of both undoped and doped samples. This occurs at 8 K in the undoped sample and 15 K in the Pt-doped sample and has approximately the same magnitude in both the doped and undoped sample. Both the fact that this

onset temperature is higher than the observed superconducting transition and the fact that it appears in both undoped and doped samples suggest that this is unrelated to the superconductivity observed in MFMMS. Varying the applied field (from 50 G to 5000 G) and repeating the low temperature portion of the measurement (Fig. 4.7c) also did not produce a superconducting response. This is not unexpected: MFMMS has been shown to be 3 orders of magnitude more sensitive than superconducting quantum interference device (SQUID) magnetometry (*18*), which is in turn more sensitive than VSM. This meant that VSM was predicted to be insufficiently sensitive to measure the superconducting transition, given that the signal-to-noise ratio of the transition observed by MFMMS was only ~50.

4.7 Discussion

While it is possible that the superconducting phase observed in the MFMMS data is novel, it is always more likely that it is a known superconducting phase. Consulting Roberts Table (*19*) indicates that the likely superconducting phase in the Pt-doped samples is $SrIr_2$, which has a recorded superconducting critical temperature of 5.7 K, the same temperature as the onset of the peak in the MFMMS data (*20*). However, in order to conclusively determine this, further study will be required. Assuming the superconducting phases is $SrIr_2$, it is unclear why this impurity phase formed only in the Pt-doped samples, since this $SrIr_2$ does not contain Pt. Whether or not this occurred by chance (due to small variances in the mixed powder sample), or some sort of catalytic effect is unknown. Moreover, because the sample was made by mixing $SrCO_3$, IrO_2 and a dopant, it is not clear how a phase could have completely reduced, since the sample is baked in a partially oxygen atmosphere.

There exists the possibility that the superconducting phase is a Pt-doped Sr_2IrO_4. This could be true if $Sr_2Ir_{1-x}Pt_xO_4$ was superconducting at the observed temperatures only within a

narrow range of Pt-concentrations. The inhomogeneous products of the powder metallurgy synthesis could produce minority phases $Sr_2Ir_{1-x}Pt_xO_4$ with a range of Pt-concentrations. If such a minority phase were superconducting, that would fit the data, though this data is insufficient to reach this conclusion. Further work will be required to isolate the superconducting phase observed in this study.

While it is not yet possible to conclusively identify the superconducting phase observed in the MFMMS data, this study demonstrates the advantages of MFMMS, when used to measure inhomogeneous samples. The sensitivity of MFMMS can be critical for detecting minute superconducting phases within larger samples, since these phases sometimes cannot be detected by magnetic measurements, as in this case. This shows that MFMMS is an ideal first screening technique, though as in this case, further study is needed in order to fully characterize these inhomogeneous samples.

4.8 Acknowledgements

Chapter 4 was prepared based on coauthored unpublished material with the following author list: Wampler, James; Trastoy, Juan; Schuller, Ivan K. J. W. was the principal researcher/author for this work.

4.9 References

1. G. H. Kwei, B. Morosin, Structures of the boron-rich boron carbides from neutron powder diffraction: Implications for the nature of the inter-icosahedral chains. *J. Phys. Chem.* **100**, 8031 (1996).

2. S. J. Clarke, C. W. Michie, M. J. Rosseinsky, Structure of Zr_2ON_2 by neutron powder diffraction: The absence of nitride-oxide ordering. *J. Solid State Chem.* **146**, 399 (1999).

3. J. de la Venta, A. C. Basaran, T. Grant, A. J. S. Machado, M. R. Suchomel, R. T. Weber, Z. Fisk, I. K. Schuller, Methodology and search for superconductivity in the La–Si–C system. *Supercond. Sci. Technol.* **24**, 075017 (2011).

4. P. C. Canfield, Fishing the Fermi sea. *Nat. Phys.* **4**, 167 (2008).

5. J. G. Bednorz, K. A. Müller, Possible High T_c Superconductivity in the Ba-La-Cu-O System. *Zeitschrift für Phys. B*. **64**, 189 (1986).

6. Y. Kamihara, H. Hiramatsu, M. Hirano, R. Kawamura, H. Yanagi, T. Kamiya, H. Hosono, Iron-based layered superconductor: LaOFeP. *J. Am. Chem. Soc.* **128**, 10012 (2006).

7. Y. Kamihara, T. Watanabe, M. Hirano, H. Hosono, Iron-based layered superconductor $La[O_{1-x}F_x]FeAs$ (x= 0.05-0.12) with T_c = 26 K. *J. Am. Chem. Soc.* **130**, 3296 (2008).

8. J. Nagamatsu, N. Nakagawa, T. Muranaka, Y. Zenitani, J. Akimitsu, Superconductivity at 39 K in Magnesium Diboride. *Nature*. **410**, 63 (2001).

9. A. P. Drozdov, M. I. Eremets, I. A. Troyan, V. Ksenofontov, S. I. Shylin, Conventional superconductivity at 203 kelvin at high pressures in the sulfur hydride system. *Nature*. **525**, 73 (2015).

10. I. N. Bhatti, A. K. Pramanik, Insight into the magnetic behavior of Sr_2IrO_4: A spontaneous magnetization study. *Phys. Lett. Sect. A Gen. At. Solid State Phys.* **383**, 1806 (2019).

11. M. K. Crawford, M. A. Subramanian, R. L. Harlow, J. A. Fernandez-Baca, Z. R. Wang, D. C. Johnston, Structural and magnetic studies of Sr_2IrO_4. *Phys. Rev. B*. **49**, 9198 (1994).

12. F. A. Wang, T. Senthil, Twisted hubbard model for Sr_2IrO_4: Magnetism and possible high temperature superconductivity. *Phys. Rev. Lett.* **106**, 2 (2011).

13. Y. K. Kim, N. H. Sung, J. D. Denlinger, B. J. Kim, Observation of a d-wave gap in electron-doped Sr_2IrO_4. *Nat. Phys.* **12**, 37 (2016).

14. Y. Klein, I. Terasaki, Insight on the electronic state of Sr2IrO4 revealed by cationic substitutions. *J. Phys. Condens. Matter*. **20**, 295201 (2008).

15. K. Momma, F. Izumi, VESTA 3 for three-dimensional visualization of crystal, volumetric and morphology data. *J. Appl. Crystallogr.* **44**, 1272 (2011).

16. C. L. Mcdaniel, S. J. Schneider, Phase Relations in the SrO-lrO_2-lr System in Air. *J. Res. Natl. Bur. Stand. - A. Phys. Chem.* **75**, 185 (1971).

17. ICSD - Inorganic Crystal Structure Database. *FIZ Karlsruhe - Leibniz Inst. Inf. Infrastruct.* (1998), (available at http://www2.fiz-karlsruhe.de/icsd_home.html).

18. J. G. Ramírez, A. C. Basaran, J. de la Venta, J. Pereiro, I. K. Schuller, Magnetic field modulated microwave spectroscopy across phase transitions and the search for new superconductors. *Reports Prog. Phys.* **77**, 093902 (2014).

19. B. W. Roberts, Survey of superconductive materials and critical evaluation of selected properties. *J. Phys. Chem. Ref. Data*. **5**, 581 (1976).

20. E. A. Wood, V. B. Compoton, Laves-Phase Compounds of Alkaline Earths and Noble

Metals. *Acta Crystallogr.* **11**, 429 (1958).

Chapter 5 – Conclusion and Outlook

The field of high temperature superconductivity has progressed slower than scientists predicted in the wake of the heady promises of the discovery of the cuprates (*1*). One fundamental limitation is that we still do not have a thorough theoretical understanding of superconductivity. Theory does not successfully predict new superconductors. Still, the last couple decades have seen the discovery of new families of superconductors, from magnesium diboride (*2*), to iron pnictides and chalcogenides (*3–6*), to the recent reports of superconducting hydrides under high pressure (*7–9*). Each new family of superconductors discovered by scientists has the potential to increase our understanding of superconductivity and to lead to game changing superconducting materials. This dissertation discussed a method of searching for new families of superconductors by measuring inhomogeneous samples with a range of material phases. And while discerning readers might note that no novel high temperature superconductors were discovered in this work, this is not unusual for this field. Significant discoveries in high temperature superconductivity have been incredibly rare and discoveries of new superconducting families have rarely been predicted by theory. Metaphorically, instead of trying to pick the perfect ticket in this lottery, this dissertation proposes a method of buying a lot of tickets.

Chapter 2 of this dissertation described the discovery of superconducting grains within two meteorites. Samples were quarried out of these meteorites and measured in MFMMS. When superconductivity was detected at ~6 K, they were divided into subsamples, which were measured. The most superconducting subsamples were characterized using scanning electron microscopy, transmission electron microscopy and computational methods. Using these techniques, the likely superconducting phases were identified as alloys of lead, indium and tin. While this is not a novel superconducting phase, it suggests the possibility of material naturally

in a superconducting space in its extraterrestrial environment.

Because superconductivity was found in two dissimilar meteorites, it is likely to be found in others. Searching for such samples could be a fruitful avenue of research. Specifically, finding superconductivity in a chondritic meteorite would suggest that superconductivity exists in the interstellar medium, since chondritic meteorites preserve a history of the pre-solar interstellar medium. Furthermore, some metallic superconducting compounds have been shown to have T_c over 10 K, such as Nb compounds, several A15 compounds containing V and Mo, and MgB_2 (*2*, *10*, *11*). Temperatures over 10 K are significantly more common in the universe than temperatures below it (*12–16*). Such a find would indicate that materials superconducting in their natural environment is much more common than the findings presented in this dissertation suggest.

Chapter 3 of this dissertation discussed MFMMS measurements of high quality Fe_3O_4 (magnetite) thin films. Magnetite goes through the Verwey transition (*17*) at about 120 K, which produces a MFMMS response that changes as a function of DC magnetic field. By measuring a series of isothermal magnetoresistance measurements and magnetization loops, it was possible to construct magnetic and electric functions of temperature for these films, for a range of DC magnetic fields. These functions were compared to the features observed in the MFMMS measurements to determine their origin. The peak observed at moderate fields was a result of the magnetic properties of the film, while the step function that switched signs at moderate fields was a result of the resistive properties. These functions could then be plugged into an equation to calculate a MFMMS signal, which could be compared to the experimental result. (*18*)

This technique has the potential to greatly increase the understanding of the MFMMS response of non-superconducting electromagnetic phase transitions. Such transitions are not well

understood, and a given type of transition (eg: a ferromagnetic transition) can produce a range of MFMMS responses (*19*), depending on the other properties of the film. By using this technique to investigate the electromagnetic origin of the features observed in MFMMS responses, it would be possible to gain an increased understanding of such transitions. Because the aforementioned equations apply to metallic, non-superconducting samples, these sorts of samples are ideal candidates for measuring using this technique. It is also ideal if these samples are thin films, since it is much easier to obtain transport measurements of such samples. Gaining a more thorough understanding of magnetic transitions in the MFMMS would make using this technique much more efficient, especially for measuring inhomogeneous samples. This is because it would be possible to efficiently characterize phase changes within the MFMMS without needing to rely on other techniques.

Chapter 4 of this dissertation discussed the search for superconductivity in chemically doped Sr_2IrO_4 powder samples. While superconductivity was detected in Pt-doped samples, it is likely that the superconducting phase is $SrIr_2$, a known superconductor (*20*, *21*). In order to confirm this, it will be necessary to synthesize $SrIr_2$ and compare the MFMMS response of this sample to that of the Pt-doped Sr_2IrO_4. Divide and conquer may also be necessary, depending on the results of this study. If it is determined that the superconducting response results from $SrIr_2$, this presents an additional question: it is unclear why this phase would form in only Pt-doped samples. Further research will be needed to answer these questions.

While this thesis presents several methods for investigating inhomogeneous samples with MFMMS and several projects involving these techniques, it does not include any work studying phase spread alloys. While there is at least one previous report on this topic (*22*), there is

potential for further research using this technique, due to the ease of characterization of samples produced using this method and due to the range of material phases produced using this method.

In all these methods, sample synthesis or procurement (for natural samples) is usually the limiting factor to research. That makes MFMMS an ideal technique for collaboration. The material phase space in which superconducting compounds can exist is enormous and as long as a researcher has samples to measure, MFMMS can quickly determine which materials might contain superconductivity.

1. P. M. Grant, Woodstock of physics revisited. *Nature*. **386**, 115 (1997).

2. J. Nagamatsu, N. Nakagawa, T. Muranaka, Y. Zenitani, J. Akimitsu, Superconductivity at 39 K in Magnesium Diboride. *Nature*. **410**, 63 (2001).

3. Y. Kamihara, T. Watanabe, M. Hirano, H. Hosono, Iron-based layered superconductor $La[O_{1-x}F_x]FeAs$ (x= 0.05-0.12) with T_c = 26 K. *J. Am. Chem. Soc.* **130**, 3296 (2008).

4. Y. Kamihara, H. Hiramatsu, M. Hirano, R. Kawamura, H. Yanagi, T. Kamiya, H. Hosono, Iron-based layered superconductor: LaOFeP. *J. Am. Chem. Soc.* **128**, 10012 (2006).

5. G. R. Stewart, Superconductivity in iron compounds. *Rev. Mod. Phys.* **83**, 1589 (2011).

6. Q. Si, R. Yu, E. Abrahams, High-temperature superconductivity in iron pnictides and chalcogenides. *Nat. Rev. Mater.* **1**, 1 (2016).

7. A. P. Drozdov, M. I. Eremets, I. A. Troyan, V. Ksenofontov, S. I. Shylin, Conventional superconductivity at 203 kelvin at high pressures in the sulfur hydride system. *Nature*. **525**, 73 (2015).

8. M. Somayazulu, M. Ahart, A. K. Mishra, Z. M. Geballe, M. Baldini, Y. Meng, V. V. Struzhkin, R. J. Hemley, Evidence for Superconductivity above 260 K in Lanthanum Superhydride at Megabar Pressures. *Phys. Rev. Lett.* **122**, 27001 (2019).

9. A. P. Drozdov, P. P. Kong, V. S. Minkov, S. P. Besedin, M. A. Kuzovnikov, S. Mozaffari, L. Balicas, F. F. Balakirev, D. E. Graf, V. B. Prakapenka, E. Greenberg, D. A. Knyazev, M. Tkacz, M. I. Eremets, Superconductivity at 250 K in lanthanum hydride under high pressures. *Nature*. **569**, 528 (2019).

10. D. Dew-Hughes, Superconducting A-15 compounds : A review. *Cryogenics (Guildf)*. **8**, 435 (1975).

11. B. W. Roberts, Survey of superconductive materials and critical evaluation of selected properties. *J. Phys. Chem. Ref. Data*. **5**, 581 (1976).

12. J. M. Greenberg, Interstellar Grain Temperatures. Effects of Grain Materials and Radiation Fields. *Astron. Astrophys.* **12**, 240 (1971).

13. P. Ehrenfreund, W. A. Schutte, Infrared Observations of Interstellar Ices. *Astrochem. From Mol. Clouds to Planet. Syst. Int. Astron. Union Symp.* **197**, 135 (2000).

14. P. Ehrenfreund, S. B. Charnley, Organic Molecules in the Interstellar Medium, Comets and Meteorites: A Voyage from Dark Clouds to the Early Earth. *Annu. Rev. Astron. Astrophys.* **38**, 427 (2000).

15. P. Ehrenfreund, H. J. Fraser, J. Blum, J. H. E. Cartwright, J. M. Garcã, E. Hadamcik, Physics and chemistry of icy particles in the universe : answers from microgravity. *Planet. Space Sci.* **51**, 473 (2003).

16. E. A. Bergin, M. Tafalla, Cold Dark Clouds: The Initial Conditions for Star Formation. *Annu. Rev. Astron. Astrophys.* **45**, 339 (2007).

17. F. Walz, The Verwey transition - a topical review. *J. Phys. Condens. Matter*. **14**, R285 (2002).

18. F. J. Owens, C. P. J. Poole, in *Electromagnetic Absorption in the Copper Oxide Superconductors* (Kluwer Academic Publishers, New York, Boston, Dordrecht, London, Moscow, 1999), pp. 75–84.

19. J. G. Ramírez, A. C. Basaran, J. de la Venta, J. Pereiro, I. K. Schuller, Magnetic field modulated microwave spectroscopy across phase transitions and the search for new superconductors. *Reports Prog. Phys.* **77**, 093902 (2014).

20. B. T. Matthias, E. Corenzwit, Superconducting Alkaline Earth Compounds. *Phys. Rev.* **107**, 1558 (1957).

21. E. A. Wood, V. B. Compoton, Laves-Phase Compounds of Alkaline Earths and Noble Metals. *Acta Crystallogr.* **11**, 429 (1958).

22. J. de la Venta, A. C. Basaran, T. Grant, A. J. S. Machado, M. R. Suchomel, R. T. Weber, Z. Fisk, I. K. Schuller, Methodology and search for superconductivity in the La–Si–C system. *Supercond. Sci. Technol.* **24**, 075017 (2011).